MODELING AND CONTROL OF CONTINUOUS TUMBLE MIXING OF GRANULAR MATERIALS

By

Andrés F. Valencia

A thesis submitted in partial fulfillment of the requirements for the degree of

MASTER OF SCIENCE
in
CHEMICAL ENGINEERING

UNIVERSITY OF PUERTO RICO
MAYAGÜEZ CAMPUS
June, 2005

Approved by:

_____	_____
Dr. Carlos Velázquez Figueroa, Ph.D. President, Graduate Committee	Date
_____	_____
Dr. Moses N. Bogere, Ph.D. Member, Graduate Committee	Date
_____	_____
Dr. Fernando J. Muzzio, Ph.D. Member, Graduate Committee	Date
_____	_____
Dr. Eduardo Juan García, Ph.D. Representative of Graduate Studies	Date
_____	_____
Dr. Nelson Cardona Martínez, Ph.D. Chairperson of the Department	Date

ABSTRACT

An approach to automatic control of a continuous tumble mixer of powders is presented. The control system is based on an ideal model that describes the mixer dynamics where the controlled variables are the outlet flow from the mixer and the variance of mixing, while the manipulated variables are the inlet flow of material to mix, with a predetermined ratio of compounds A and B, and the rotational velocity of the mixer. The system illustrates a *Multi Input Multi Output* (MIMO) control problem, where each manipulated variable affect both controlled variables. A strategy of two feedback PI controllers was successfully implemented, and it was compared to an MPC strategy: The simulations results provided an excellent tool to compare and study stability, effects of overshoots on set-point tracking, performance, robustness and the capacity to reject the effect of load disturbances.

RESUMEN

Una propuesta para el control automático de un mezclador continuo giratorio de polvos es presentado a continuación. El sistema de control está basado en un modelo ideal que describe la dinámica de mezclado, en el cual las variables controladas son el flujo de salida de material y la varianza de mezclado, mientras las variables manipuladas son el flujo de entrada de material, con una relación predeterminada de compuestos A y B, y la velocidad de rotación del mezclador. El sistema ilustra un problema de control *Múltiples Entradas Múltiples Salidas* (MIMO), donde cada variable manipulada afecta las dos variables controladas. Una estrategia de dos controladores PI *feedback* fue implementada y comparada con una estrategia MPC: Los resultados obtenidos por simulación fueron la herramienta usada para comparar y estudiar estabilidad, efectos de sobrepasos por cambios en *set-point*, desempeño, robustez y capacidad para contrarrestar los efectos de perturbaciones.

This thesis is dedicated to Fernando and Nikolas… my two best friends.

TABLE OF CONTENT

LIST OF TABLES

LIST OF FIGURES

CHAPTER I: INTRODUCTION

I.1 Justification

Pharmaceutical companies have developed extensive research programs in drug delivery, but much less effort has been devoted to the technology used to manufacture drug products. Most of the operations in the manufacturing process are *powder technologies* where, for more than thirty years, the methods of production and control strategies have not changed significantly.

Typical operations in the manufacture of powder drug products, such as mixing, granulation, milling, drying, and others, are *batch operations*. When these operations are subjected to control activities and functions that provide process finite quantities of input materials and an ordered set of processing activities over a finite period of time using one or more pieces of equipment, the operations are under *batch control*.

Due to economic trends and social impacts, pharmaceutical product manufacturing is in serious need of technical upgrading [1]. Moving from batch to continuous operations of manufacturing systems is an option that is being considered by *U. S. Food and Drug Administration* (US FDA) and research groups. In powder mixing, the change from batch to continuous mixers is prompted by the availability of instrumentation and simplified production scheme [2].

In the field of control focused to powder mixing, the batch control is the tool implemented following the recommendations of ISA-88 ISA Batch Systems Standards [3]. No previous open literature was presented, to the best knowledge of the author, in control of continuous powder mixing, perhaps due to the absence of dynamic models of mixing. For continuous powder drug mixing processes where the controlled variables are the flow of mixed material and its variance, the control strategies should insure a stable operation, execution of accurate ranges, removal of effects of dead time, predict the effects of load disturbances, avoid excessive overshoots on set-point tracking, and other

common characteristics of performance and safety in order to comply with established governmental regulations and laws.

A direct synthesis tuning method for a *Proportional Integral* (PI) controller of mixing should produce smooth closed-loop response with strong robustness, without modifying the original structure into this controller. However, the measure of the variance in the flow of mixed material is obtained using on-line image analysis involving dead time. Many schemes have been suggested to remove the detrimental effects of dead time on close-loop stability and feedback control [4].

Advanced control strategies like *Model Predictive Control* (MPC) are introduced to move the process variables dynamically for productivity improvement, utility cost reduction, and quality control as was summarized by Seborg *et al*. [5]. The main advantages of MPC are: (1) the control strategy is suitable for non-linear processes with long delay; (2) the control performance is optimized by on-line optimizer, (3) prevent violations of input and output constraints, and (4) the process model and control strategy can be updated on-line to compensate for changes in the process conditions. This strategy begins to prevail in industrial environment for difficult process where it is necessary to reach high levels of performance and robustness.

I.2 **Objectives**

The main objective is to determine the best control strategy for a continuous rotating powder mixer. Specific objectives include to:

- Develop an ideal model to describe a continuous rotating powder mixer.
- Develop two feedback control strategies (PI, MPC) for a continuous rotating powder mixer, where the mixer dynamics is described by the model developed above.
- Compare the robustness, overshoots on set-point tracking, performance and capacity to reject the effect of load disturbances of the strategies developed.

CHAPTER II: BACKGROUND AND LITERATURE REVIEW

II.1 Background

Powder mixtures can be classified into two major groups, one that involves free-flowing particles and the other containing cohesive or interactive constituents. A free-flowing mixture will generally permit individual particles to move independently or freely, while a cohesive mixture generally has some interparticulate bonding mechanism, permitting particles to move only with an associated cluster of particles.

The formation of a mixture involving only free-flowing particles is a statistical or stochastic process in which the rules of probability apply. If the free-flowing particles are identical in all aspects except color, then a completely random mixture can be obtained. If they are not identical, a partially randomized final mixture will be generated due to incomplete mixing or segregation present in the mixing process. A cohesive mixture contains one or more cohesive constituents and its final state is mainly determined by interparticulate forces.

A few studies have been conducted to model solid mixing. Significant progress has been made in the understanding of mixing and segregation of free-flowing and relatively large particles. However, mixing of cohesive powders remains largely untouched [1]. Fan *et al.* [6] conducted a review of the major developments in solids mixing from 1976 to 1990, in which they present the rates and mechanisms of mixing and they make a classification based on flow characteristic leading to random models.

Malhotra *et al.* [7] presented experimental results on the fundamental particle mixing phenomena in a bed of granular material agitated by a moving blade in a two-dimensional cylindrical vessel. The results demonstrated that the particle velocity distribution map within the bed is circular in nature and there exists a small region of very little particle movement just above the tip of the blade.

Computational studies of mixing have been performed by Kaneko *et al.* [8] in a single helical ribbon agitator demonstrating that the distance between the blade top and the bed surface is the most important parameter to attain good mixing. The mathematical model was developed based on the following assumptions for simplification:

- Particles are spherical in shape and uniform in diameter and move in a three dimensional space.
- The gas-to-particle interaction and the particle-to-particle adhesion are neglected. Forces considered are those for gravity and collisions between particles, between particle and wall and between particle and blade.
- Particles are supposed to have a soft sphere interaction expressed by a Hookean linear spring, a dash pot and a friction slider with Coulomb's law of friction.
- The spring constant is adjusted only from the viewpoint of numerical economy.

Both translational and rotational motions are considered in equations of motion into the model:

$$\ddot{\mathbf{x}} = \frac{\left(\mathbf{F}_n + \mathbf{F}_t\right)}{m} + \mathbf{g} \tag{II.1}$$

$$\dot{\omega} = \frac{\mathbf{T}_c}{I} \tag{II.2}$$

where $\mathbf{x}$ is the position vector of the center of the particle, $\mathbf{F}_n$ and $\mathbf{F}_t$ are the sum of the collisions forces respectively for the normal and tangential directions acting on colliding particles, m is the mass of particles, $\mathbf{g}$ is the gravity acceleration, ω is the angular velocity vector of a particle, $\mathbf{T}_c$ is the summation of torque caused by particle collision and I is the moment of inertia. The Euler scheme was used to integrate (II.1) and (II.2) to obtain the new velocity, position and angular velocity of a particle after a time step.

McCarthy *et al.* [9] did some computational studies of tumbler mixing, focused on two very different techniques: *Particle Dynamics* (PD) and *Lagrangian Simulation* (LS). According to the results, PD is versatile in that particle level interactions, including inelastic, frictional forces can be accounted for, such that segregation resulting from differences in particle properties can be explicitly studied. LS are based on continuum models.

McCarthy [10] also examined both computationally and experimentally a micro-modeling of cohesive mixing process, where it was established that mixing is enhanced only slightly at intermediate levels of cohesion in wet systems.

Aoun-Habbache *et al.* [11] developed the simultaneous axial and radial model for mixing of particles in a hoop mixer in the absence of segregation effects, based on image analysis of photographs of sections taken at different depths of the mixer. The results showed that the particles located at the bottom and in the central part of the mixer can experience higher mobility than the others, and consequently enhance the mixing kinetics.

II.2 **Mixing of granular materials in circular rotating containers**

A tumbler refers to any hollow vessel which is partially filled with granular material and rotates, so that a circulating flow is produced. Tumblers exhibit different flow regimes (avalanching, slumping, rolling, cascading, raining, and centrifuging), depending on the rotational speed.

McCarthy *et al.* [12] presented a model of granular mixing developed using experimental pictures of mixing in simple tumblers in a variety of 2-D mixer geometries. The materials to mix were two similar and noncohesive granular powders, that is, the particle's diffusivity was small. His work was focused primarily on the simplest regime, from the viewpoint of mixing and granular flow: *the avalanching regime*. In this regime each avalanche completes its descent before another avalanche begins. When a granular

material exceeds its maximum angle of stability (left in Figure II.1), an avalanche occurs and the surface relaxes to the material's angle repose (right in Figure II.1). When this avalanche occurs, the dark gray material moves from the top of the surface to the bottom as shown.

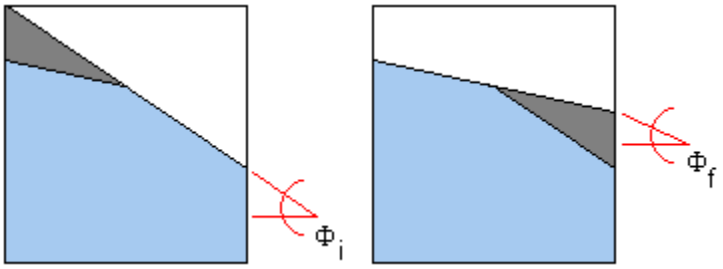

Figure II.1 Movement of a wedge of material [12].

For problems involving the mixing of two similar, noncohesive powders, where they differ only in color, geometrical effects dominate and the mixing within a wedge is well described by one of the simplest wedge dynamics [12]. The most straightforward use of this approach is to study mixing in uniformly-convex 2-D containers such as a cylinder. In this geometry, the material is allowed to fall freely down the surface and the location of the avalanching material both before and after the avalanche is easily determined by a differential balance, with the additional constraint that the bed density remains constant.

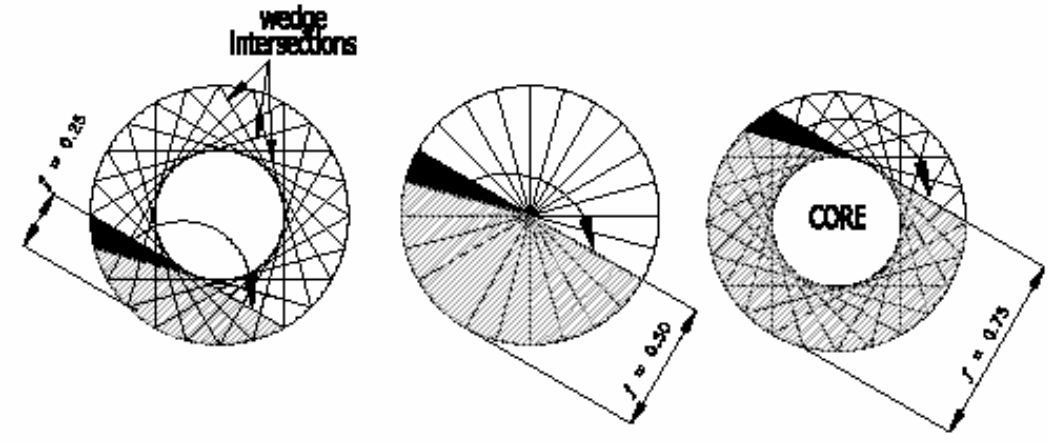

Figure II.2 Motion of wedges in a circle tumbling mixer [12].

Figure II.2 shows three fill levels f, 0.25, 0.50 and 0.75. During an avalanche, the dark wedge falls to the position of the light wedge, and mixing occurs. For $f = 0.25$ the material in one wedge will enter a new wedge upon further rotation, enhancing interwedge mixing. There are no wedge intersections for $f = 0.50$. For $f = 0.75$ appears the formation of a core, that is, centrally located material which never participates in an avalanche and therefore never mixes.

Elperin *et al.* [13] did a study using a kinematic approach for the mixing of granular material in a two-dimensional slowly rotating container. The model aims at estimating the mixing capacity of a mixer when the particles diffusivity is small. In this study, it was considered a two-dimensional convex mixer partially filled with a granular material with constant bulk density. The container slowly rotates around a horizontal axis with a constant angular velocity $\dot{\varpi} = 1$. Thus, the angle of rotation can be used instead of the time variable. The free surface of the granular material bed is supposed to be flat and it is inclined at a constant angle of repose. The height of the free surface is $z = h(\varpi)$. Each particle rotates with the bulk of the material and when it reaches the free surface it falls down and sediments at the bulk at a new position. When a container with volume V_0 is filled with granular material occupying a volume V, the mixing efficiency μ is defined as the product of the mean deformation per unit volume of the avalanching material, in function of stretching rate λ and the length of the free surface L, and the filling level of the granular material in a mixer $f = V/V_0$:

$$\mu = f \frac{\int_0^{2\pi} |\lambda| \frac{L^2}{2} d\varpi}{V} \tag{II.3}$$

The simulated and experimental results obtained by McCarthy *et al.* and the analytical results obtained by Elperin *et al.* are similar. For any fill level, a diagram can be drawn to follow the motion of a wedge of material as it travels clockwise from its original position to its avalanche position, as is shown in Figure II.2. This demonstrates

the importance of the fill level. At low fill levels, there are many wedge intersections, so a share of any wedge eventually finds itself being part of another wedge, thus enhancing interwedge mixing. However, as the fill level increases, the mixing goes through a maximum. As the length of material increases no wedge of material can mix with any other wedge since their intersections decreasing the mixing. When the fill level reaches specifically above the center of mass of the mixer throughout the entire rotation, the mixing arrives to its minimum. From this fill level on, occurs the core formation, where the wedges do not encompass the entire breadth of the material, generating a region of material, called core, that does not get included in the avalanching process. When the container is full, no avalanching can occur and the mixing stops. Figure II.3 shows the mixing efficiency in a two-dimensional mixer with a circular cross-section [12-13].

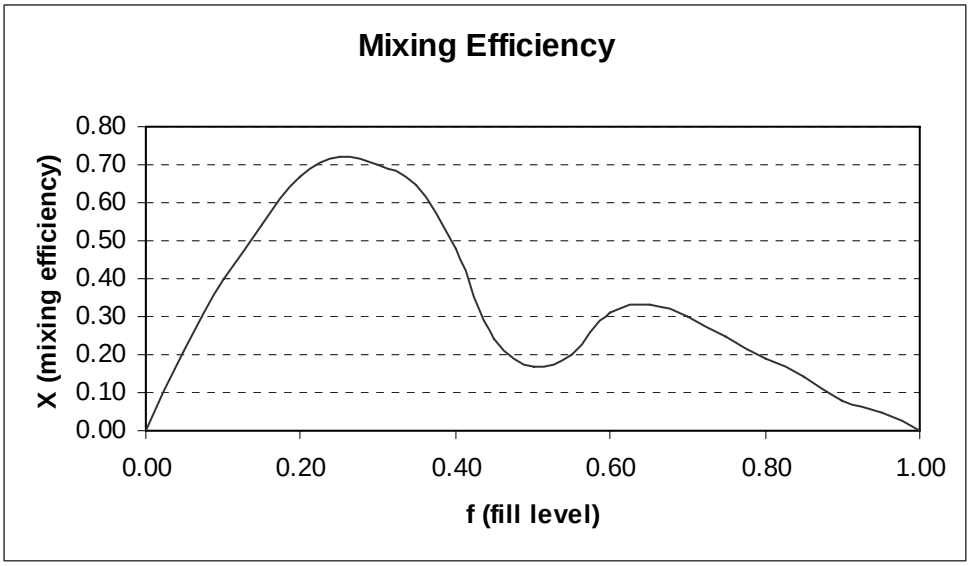

Figure II.3 Mixing efficiency in a 2-D mixer with a circular cross-section [11].

McCarthy *et al.* [12] also described the case of the three-dimensional geometries for rotating containers, where the wedge shapes vary in a complex way, but the same idea of the two-dimensional geometry is hold: avalanches move material from the upper portion of the surface to the lower, and mixing within the wedge of material occurs only during the avalanche. Basically, the radial mixing, that is, mixing perpendicular to the axis of rotation of the mixer, is described in the same form that in the two-dimensional.

II.3 **Simulation of granular mixing in a rotating tumble**

McCarthy *et al.* [9] developed, based on continuum mechanics studies in rolling regime, where the rotation of a tumbler results in a flow of particles from the fixed bed into the cascading layer in the uphill half of the surface and a flow from the layer into the fixed bed in the downhill half. Lagrangian Simulation (LS) of the particle motion within a rotating tumbler, requires the velocity and layer thickness profiles for the flowing layer. Referring to Figure II.4, they used a macroscopic balance approach to obtain the velocity and the layer thickness. Within the layer, the components of the velocity at any point, v_x and v_y, respectively, are given by:

$$v_x = \frac{dx}{dt} = 2u\left(1 + \frac{y}{\delta(x)}\right) \tag{II.4}$$

$$v_y = \frac{dy}{dt} = -x\left(\frac{y}{\delta(x)}\right)^2 \tag{II.5}$$

where y is the coordinate perpendicular to the free surface, x is the coordinate parallel to the free surface, $\delta(x)$ is the layer thickness, t is the time, and u is the average velocity within the layer, which is roughly constant.

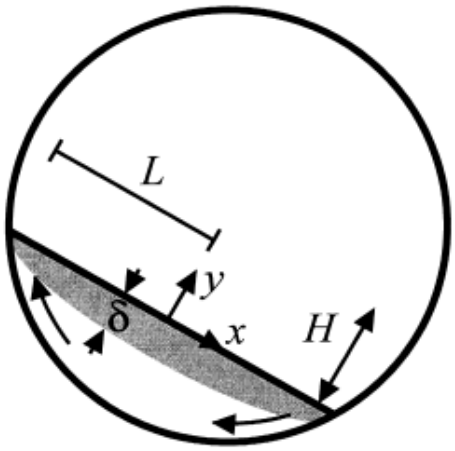

Figure II.4 Schematic representation of a cylindrical tumbler used by McCarthy *et al.* [9].

They placed identical particles of different colors, sugar crystals (SC) and sugar ball (SB), in two halves of a short cylinder using a separator. The separator was removed, the cylinder was mounted on the rollers and rotated, and digital images were recorded at short time intervals as the mixing progressed. Figures II.5 and II.6 shows the results obtained respect to the time evolution of the mixed state for two mixing experiment and the variation in the intensity of segregation I_s, respectively.

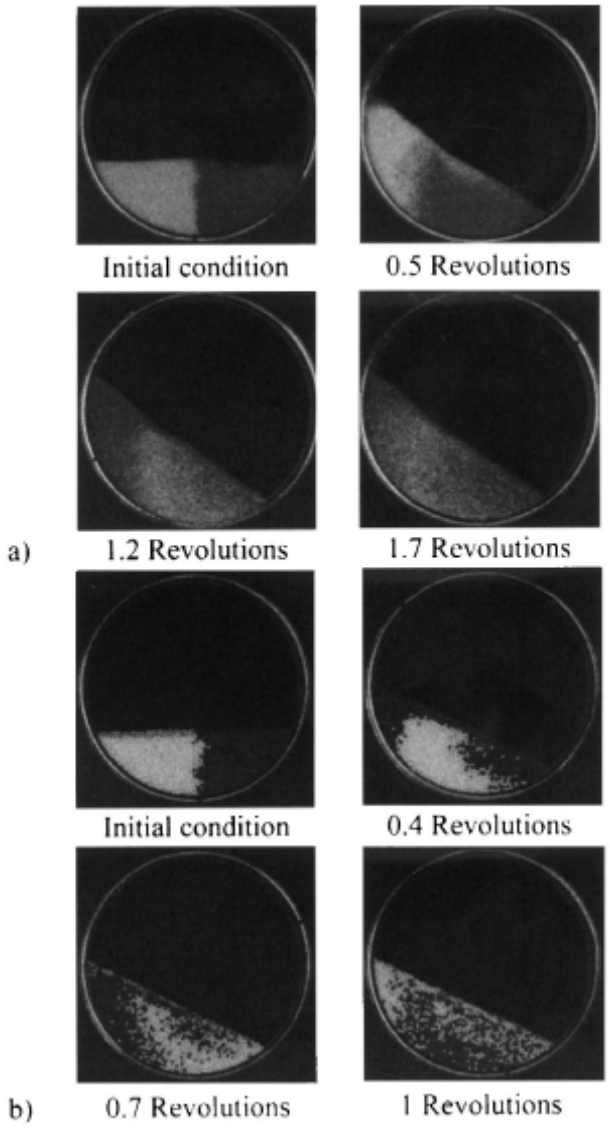

Figure II.5 Experimental time evolution of the mixing process for two differing materials: (a) Sugar crystals (SC) filled to H=0.35. (b) Sugar balls (SB) filled to H=0.42 [9].

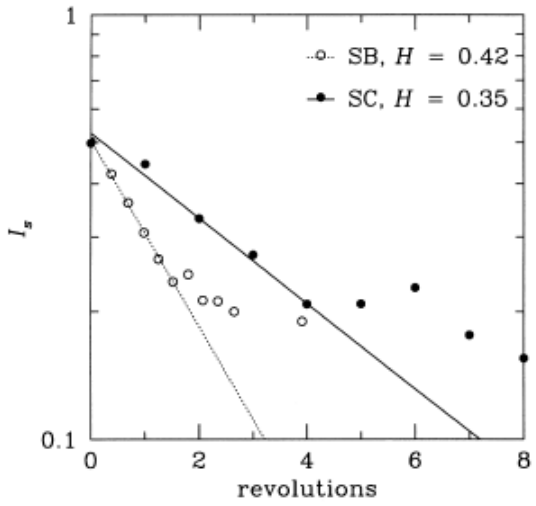

Figure II.6 Experimental intensity of segregation I_s evolution. Sugar crystals (SC) filled to H=0.35 and Sugar balls (SB) filled to H=0.42 [9].

Moakher *et al.* [14] experimentally validated computations of flow, mixing and segregation of non-cohesive grains in two types of three dimensional tumbling blenders: double-cone and V. Their results are shown in Figures II.7 and II.8. They made a quantification of the mixing rate for three upper insets, plotting the concentrations of the outermost (light gray), central (gray) and innermost (black) particles as a function of axial position after 1, 3 and 6 revolutions of the tumblers. These fits show an exponential trend between the variance of mixing and the number of revolutions of the mixer. Similarly, after a segregation study in both tumblers, they demonstrated that the intensity of segregation has the form:

$$I = I_0 - Ae^{-kN} \tag{II.6}$$

where N represents the number of revolutions, I_0 the initial segregation value, A and k are constants.

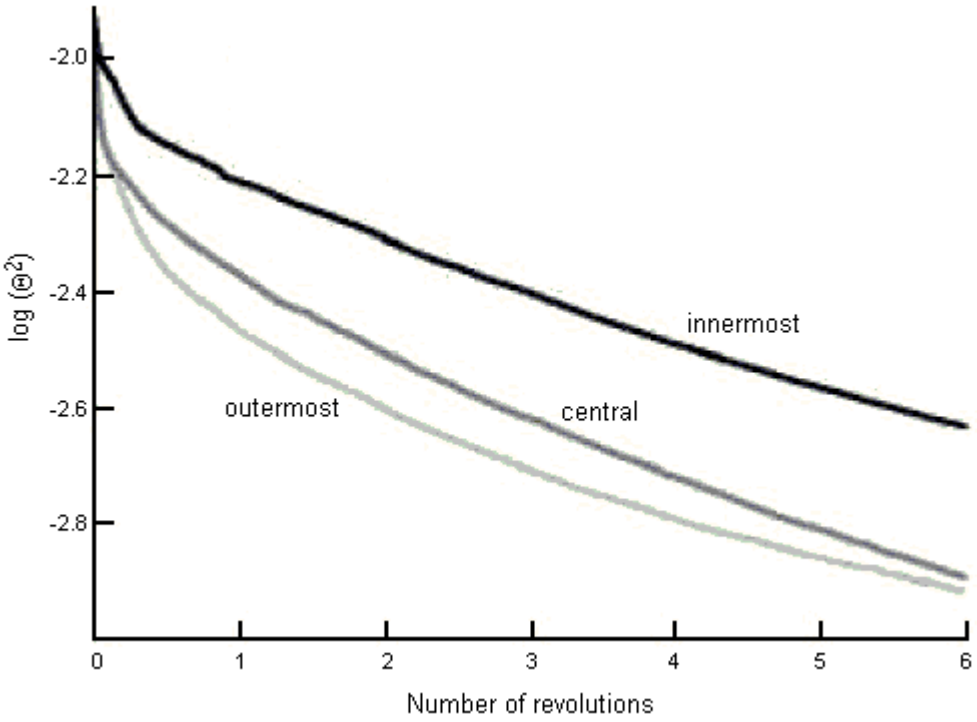

Figure II.7 Trend of the variance of volume elements in double-cone blender as a function of time [14].

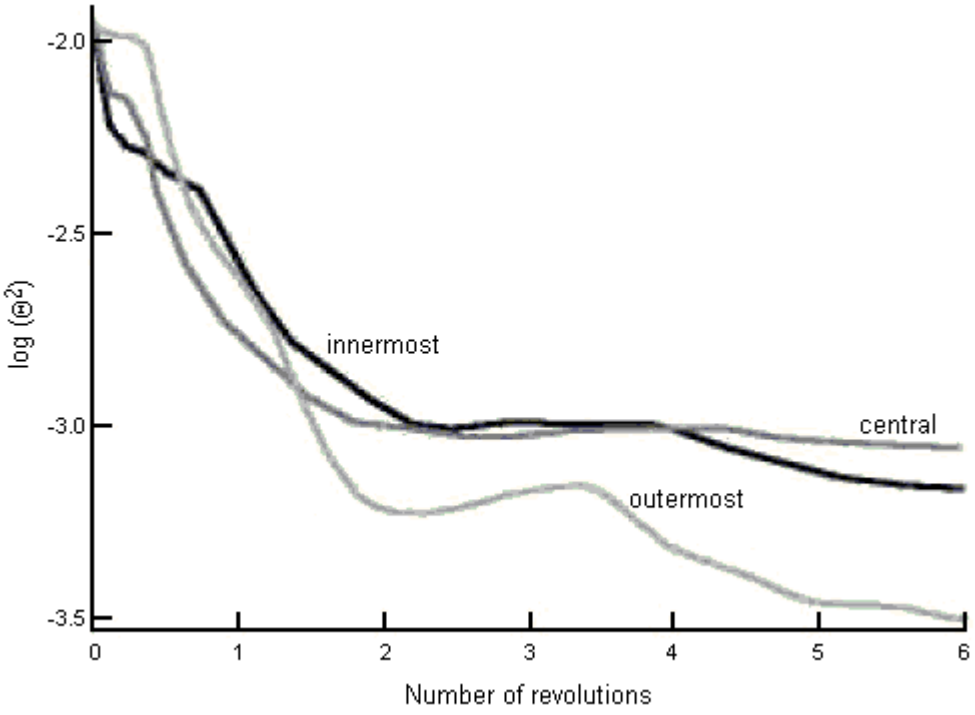

Figure II.8 Trend of the variance of volume elements in V-blender as a function of time [14].

II.4 **Continuous mixing**

An industrial continuous mixer, as an *Ajax LunFlow*™ [15], operates on a small cross section of product that, in principle, contains the correct ratio of the required final make-up. The machine function is to successively replicate a disturbance process that re-organises the bulk, to progressively increase the degree of *disorder* until suitable homogeneity is obtained. This is more efficient than employing significant axial sections to convey only and concentrating the work input by opposing the product transfer at a small region. Fixed blades are more secure for production use, although adjustable blades may be employed for test purposes.

Two main techniques are used to achieve a cross sectional mix, according to the nature of work input needed to secure the appropriate condition. To blend fine powders that are not very cohesive it is usual to run the machine at a fast speed to induce a high degree of dilate agitation. This action separates the particles and allows the different components to diffuse in the mass. The corresponding cross sectional loading of the machine is relatively low. Paddle type blades are usually used in this mode.

More intensive effort is required to merge cohesive powders mixtures. In this case the machine is run at a higher cross sectional fill so that the blades shear the product in a confined state and thereby induce higher stresses to affect the dispersion.

It should be recognized that continuous mixers may have to accommodate short-term variations in the output of the component feeders. A continuous system cannot compensate for a protracted deficiency of an ingredient but can deal with fluctuations of a cyclic or erratic nature if the average output within a short period falls within acceptable bounds.

CHAPTER III: SEMI-EMPIRICAL MODELS OF A CONTINUOUS TUMBLE MIXER

III.1 Goal of the semi-empirical models

The biggest hindrance to understanding of powders mixing is that there is no accepted set of governing equations, in part, to the difficulty in experimentally measuring the bulk properties, which would be necessary in a continuum description of a granular flow. In the previous chapter, the dynamics models and simulations of mixing processes proposed by different investigators was presented. These models were based on batch processes, where the mixer is charged with a definite quantity of material to mix and after some time is discharged.

It was demonstrated that even simple geometrical considerations can provide very helpful information about the characteristic mixing time and the optimal filling level of a circular mixer [13], while noncircular mixers are presented in terms of Poincaré sections and blob deformation, demonstrating the chaotic characteristics of these systems [16]. For the circular mixers, the geometrical considerations are based mainly on the following assumptions:

- The powder particles are spherical and their adhesion is neglected.
- The flow inside the mixer exhibits an *avalanching* regime.
- The particles diffusivity is small, this is, the powders to mix are noncohesive granular and have similar characteristics.
- The density of the powders A and B to mix are similar and the bulk density remains constant.

An objective of this research is to propose and validate a semi-empirical model that describes, accurately, the continuous mixing process of powders. This model showed approximate the dynamics of a continuous rotating mixer whose input variables will be the inlet flow of material to mix, with a predetermined ratio of compounds A and B, and

the rotational velocity of the mixer. The output variables will be the material outlet flow from the mixer and the variance of mixing. The schematic of the continuous circular mixer is presented in the Figure III.1.

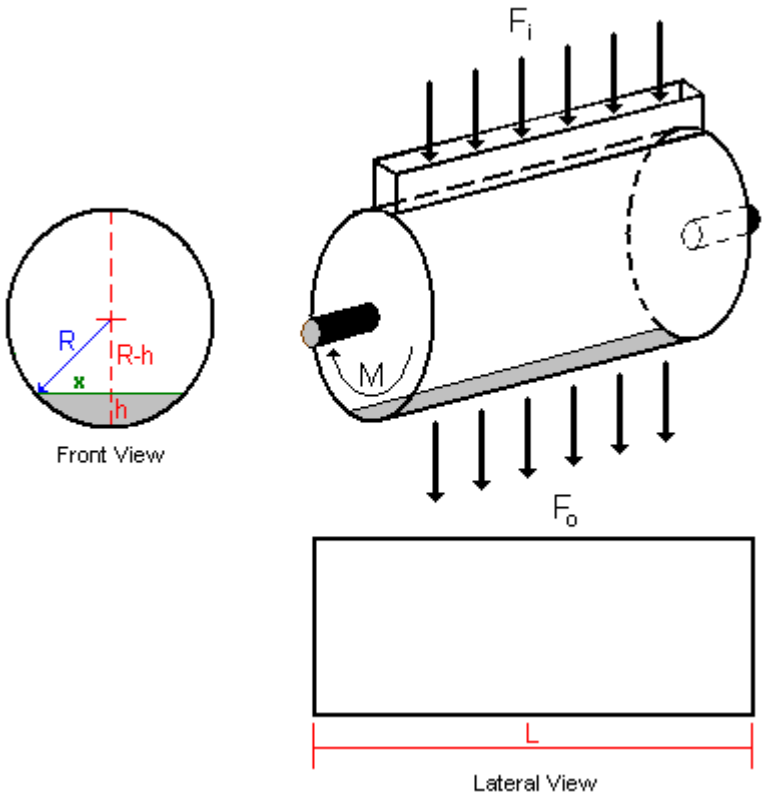

Figure III.1 Schematic of a circular mixer.

III.2 **Model of fill level in a circular rotated mixer**

No previous works have been reported in the open literature, to the best knowledge of the author, on powder mixing flow in a continuous mixer. The study of powder flow within a mixer is a rigorous problem of transport phenomena that involves contact between different solid phases. For this, a first approach to understanding granular mixing, should consider the liquid mixing problem [12], and consequently, to model the variation of fill level inside the mixer as if it were a liquid. The fill level depends on the total amount of noncohesive granular materials that is being mixed; thus, respect to Figure III.1 where the front view is an approximation when the mixer is stopped, the conservation equation selected is an overall material balance on the system:

$$\frac{dm}{dt} = \rho F_i - \rho F_o \tag{III.1}$$

An acceptable assumption [13] is that the densities of noncohesive granular materials are similar and they remain constant during the mixing process and, similar to the avalanching regime for mixing, the surface of powders inside the mixer is assumed flat at all time. The geometrical construction in Figure III.1 indicates that *x* is the length of one side of a right triangle whose hypotenuse is *R*. Thus, *x* is related to the level *h* by:

$$x^2 + (R - h)^2 = R^2 \tag{III.2}$$

$$x = \sqrt{2Rh - h^2} \tag{III.3}$$

The mass accumulation term in Eq. (III.1) can also be written as:

$$\frac{dm}{dt} = \rho \frac{dV}{dt} = \rho 2xL \frac{dh}{dt} \tag{III.4}$$

where *2xL* represents the changing surface area of the powders. Substituting Eqs. (III.3) and (III.4) in (III.1) and simplifying one obtains:

$$\frac{dh}{dt} = \frac{F_i - F_o}{2L\sqrt{2Rh - h^2}} \tag{III.5}$$

Eq. (III.5) represents the variable fill level in the circular mixer, where F_i and F_o are the inlet and outlet flows, respectively, *R* and *L* are the radius and the length of the mixer, respectively.

If the mixer is stopped, as in Figure III.1, the gravity flow of bulk solids occurs under the pressure corresponding to the equivalent of a *static head of the material*. Such

head would be caused by the height of a solid column in a bin, but in practice is often not available to produce the flow due to phenomena known as *arching* or *bridging*. The velocity head at the discharge from the bin is usually a small fraction of the head, with the major part being consumed by the friction of the moving solids against the walls of the bin, as well as against similar solids. The friction force is tangent to the surfaces of contact of the two bodies and always opposes motion. The coefficient of static friction μ for any two surfaces is the ratio of the limiting friction to the corresponding normal pressure:

$$\mu = \frac{F}{N} \tag{III.6}$$

where F is the maximum friction of impeding motion and N is the normal pressure. If a body rest on an inclined plane and if the angle of inclination of the plane to the horizontal, α, is such that motion of the body impends, this angle α is defined as the angle of repose, so it follows that:

$$\mu = \tan\alpha \tag{III.7}$$

As an approximation, the outlet flow of mixed powder F_o depends only on the mechanical adjustment at the bottom of the mixer. For modeling effects, it is assumed that the mixed powder outlet flow behaves in a similar way to flow rate through an orifice[1], according to:

$$F_o = K_o\sqrt{h} \tag{III.6}$$

where h represents the fill level of powder inside the mixer and K_o the flow constant [$L^{(5/2)}$/t]. The substitution of Eq. (III.6) into (III.5) gives:

[1] This relation is derived from a mechanical energy balance or *Bernoulli equation*. In the practice, this relations type for a circular mixer could be approximated making a calibration procedure over mechanical equipment, measuring the powder mixed flow out as function of the fill level into the mixer.

$$\frac{dh}{dt} = \frac{F_i - K_o\sqrt{h}}{2L\sqrt{2Rh - h^2}} \tag{III.7}$$

Eq. (III.7) represents the change in the fill level inside the mixer if the mixer is stopped, this considering an approximation in the powders physics similar to a *Newtonian fluid*.

As it is shown in Figures II.2, II.4, II.6 and III.2, the flat surface is displaced in direction of the rotation of the mixer. Khakhar *et al.* [16] found that when the mixer is half full, the entire bed passes through the layer in half a revolution of the mixer, so that the volumetric flow per unit cylinder length calculated at the midpoint of the layer ($x = 0$) is:

$$Q_0 = \frac{\pi L^2}{2}\frac{1}{(\pi / M)} = \frac{ML^2}{2} \tag{III.8}$$

where L is the length scale of the system and M the rotational velocity of the mixer.

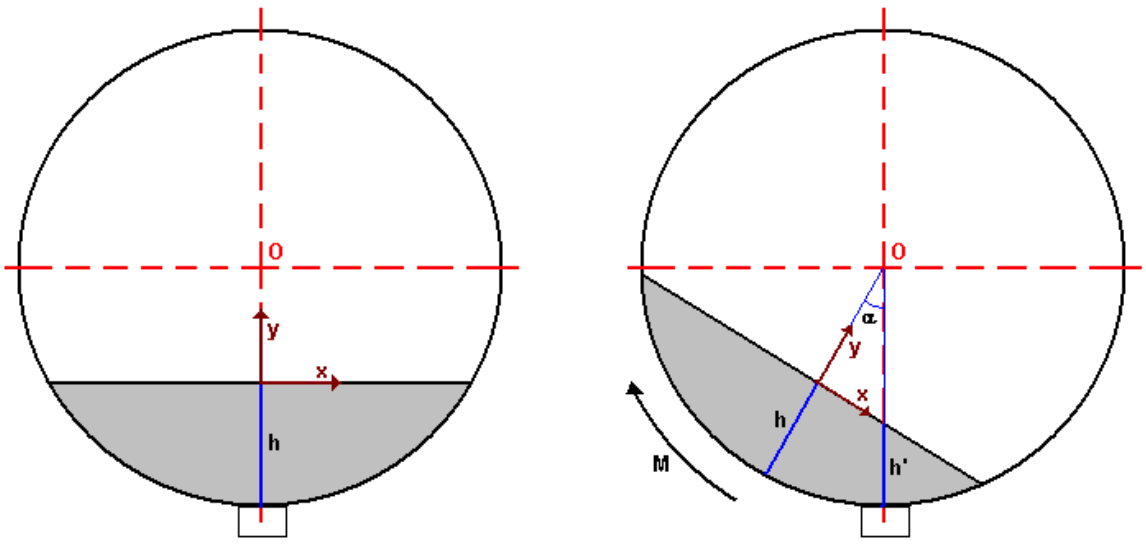

Figure III.2 Dynamics of a circular mixer view. (a) Mixer stopped. (b) Mixer rotating.

The behavior of the mixing depends of the operating regime, which may be quantified in terms of the *Froude number*. The Froude number represents the proportion between the inertial force and gravitational force, and is used in momentum transfer in general and open channel flow and wave and surface behavior calculations in particular. It is normally defined as:

$$Fr = \frac{M^2}{gL} \tag{III.9}$$

At low speeds or low Froude number, the flow is intermittent and comprises discrete time-periodic avalanches [16]. The transverse mixing in this case is dominated by geometry. Each avalanche results in a wedge-shaped bed of particles at the free surface, abruptly cascading to form a new wedge at a lower position. At higher mixer rotational speeds, the continuous flow rolling regime is obtained, in which a thin layer of particles flows down the free surface while the remaining particles rotate as a fixed bed. Particles continuously enter the layer from the fixed bed in the upper-half of the layer, and exit from the layer into the fixed bed in the lower half; the free surface in this regime remains flat.

From the Figure III.2 (b) and rewriting mixed powder outlet flow as $F_0 = K_o\sqrt{h'}$, then $h' = f(\alpha, h)$ and $\alpha = f(M)$. Thus, the outlet flow F_o, as the mixer is rotating, can be approximated for simulation effects as a function of fill level inside and the rotational velocity of the mixer:

$$F_o = f(M, h) \tag{III.10}$$

When the rotational velocity of the mixer is very low, the outlet flow of mixed powder F_o, is approximated by Eq. (III.6), and as the rotational velocity increases, the outlet flow must decrease due to the change in the angle α and *h'*. Thus, as a first

approximation, the differential equation proposed to model the fill level *h* within a continuous mixer is given by:

$$\frac{dh}{dt} = \frac{F_i - \dfrac{K_o\sqrt{h}}{1+\beta M}}{2L\sqrt{2Rh-h^2}} \qquad \text{(III.11)}$$

where β is a constant. This suggestion is only a heuristic, yet it appears to be followed by the system simulated as will be shown later.

III.3 **Model of variance of mixing for the continuous rotated mixer**

As it was presented above, the models, experiments and simulations of segregation and variance presented in the literature were developed in batch operations in cylinders, double-cone and V-blenders. Diverse studies [8,13] evaluate the segregation rate in bidisperse systems by plotting the intensity of segregation as a function of the number of revolution, as in Figure II.6. The intensity of segregation, *I*, is defined as:

$$I = \sqrt{\frac{\sum_{i=1}^{n}(\phi_i - \phi_m)^2}{N-1}} \qquad \text{(III.12)}$$

where ϕ_i are the concentrations at the set on *N* uniformly distributed points in the bed and ϕ_m is the overall concentration. Figures II.7 and II.8 depict the exponential relation that exits between the number of revolutions of a tumbler and the variance of mixing. This type of relation can be extended to continuous mixers [14]. Figure III.3 depicts the relation as function of time found experimentally that exists between the fill level h inside the mixing and the variance of mixed. The constant k_n is a proportional function of the fill level within the mixer, this is, $k_n \propto f(h)$.

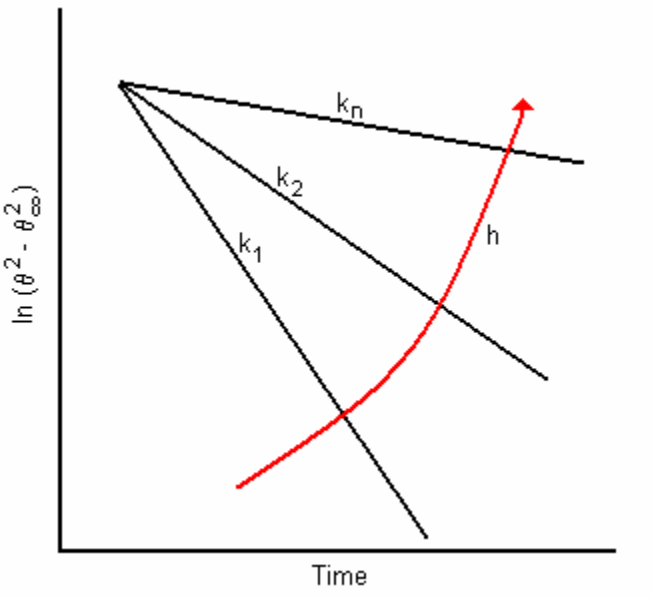

Figure III.3 Logarithmic behavior of the variance of mixing for a continuous mixer (F.J. Muzzio, 2005).

Thus, as a first approximation, the generalized model proposed to simulate the variance of mixing within a continuous mixer is given by:

$$\theta^2 - \theta_\infty^2 = Ae^{-\psi h M} \tag{III.13}$$

where A and ψ are constants, h is the fill level within the mixer and M represents the rotational velocity of the mixer.

The semi-empirical models in Eqs. (III.11) and (III.13) for outlet flow and variance respectively, are strongly nonlinear and dependent on inlet flow $F_i(t)$ and rotational velocity $M(t)$.

III.4 **Simulation of semi-empirical models**

The proposed semi-empirical models were simulated on Simulink® file, where the model in differential form, Eqs. (III.11) and (III.13), was run with a simulation time of 200 000 seconds with the following changes in the input variables:

- Load over Inlet Flow:

Table III.1 Load over inlet flow within the semi-empirical models.

Time [sec]	Final Value [cm^3/s]	Change Type
0	64	---
40 000	40	Step
170 000	---	Ramp
200 000	64	---

- Load over Rotational Velocity:

Table III.2 Load over rotational velocity within the semi-empirical models.

Time [sec]	Final Value [rps]	Change Type
0	2	---
80 000	4	Step

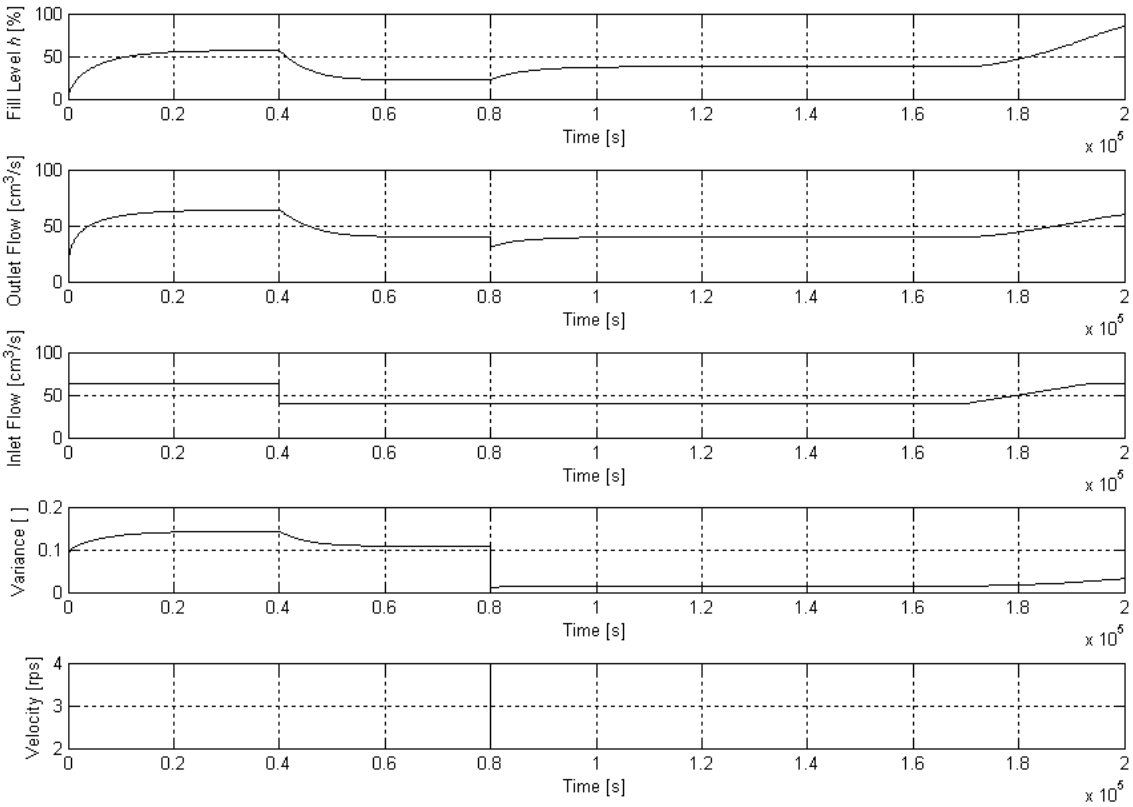

Figure III.4 Response of semi-empirical models. (a) Fill Level, (b) Outlet Flow, (c) Inlet Flow, (d) Variance, (e) Rotational velocity.

Figure III.4, shows the response of the semi-empirical models to changes in the inputs variables. When the inlet flow increases, both the variance and outlet flow increases too, this is due to the presence of greater amount of material within the mixer. Similarly, when the inlet flow decreases, the outputs variables decrease too. Finally, when the rotational velocity of the mixer increases, the variance decreases and the outlet flow decreases too. These trends in the output variables of the semi-empirical models are consistent with the expected from the physical point of view.

CHAPTER IV: MULTIVARIABLE CONTROL - PI DESIGN

IV.1 Goals of the multivariable PI control

This chapter focuses on the analysis of the continuous mixer from a control theory point of view, applying some analysis and design techniques focused on the multivariable system where the input variables are the inlet flow of material to mix and the rotational velocity of the mixer, and the output variables are the material outlet flow from the mixer and the variance of mixing.

First, the semi-empirical models in time domain were connected in Laplace domain to convert the original differential equations in a set of algebraic equations, known as *transfer functions*. Then, these transfer functions and the characteristic of a multivariable control system, were used to perform a controllability and observability analysis in terms of *state space*.

Last step was the design of two *Proportional Integral* controllers (PI) with their interactions for the control of the system in study.

IV.2 Model system development using linear regression

The time domain models previously developed are strongly nonlinear. Their transformation to Laplace domain requires many assumptions to obtain the final model, which add inaccuracies that could make the model ineffective.

An alternate approach is to develop an experimental model from an output data response to a change previously defined input and performing an analysis known as *parameter estimation* or regression.

The first step was to perform a step change in one of the process input maintaining the others constant. The second step was to obtain the model using *Design*

Tools of *Control Station Software*[1]. The fitting routine systematically searches for the model parameters that minimize the Sum of Squared Errors (SSE) between the response contained in the measured data, and the response predicted by the model being fit both to the same change in the manipulated variable data in the file. With *i* indicating any one of the *N* total data points in the set, the SSE is expressed:

$$SSE = \sum_{i=1}^{N} \left(Measured\_Data_i - Model\_Data_i \right)^2 \tag{IV.1}$$

In general, the smaller the SSE, the better the model describes the data. To obtain a meaningful fit, it was essential to recognize that the process in the original model will be at steady state before collection of dynamic data begins and that the first data point in the file will equal the initial steady state value. The best models obtained were:

$$\frac{F_o(s)}{F_i(s)} = G_{p11}(s) = \frac{0.9908}{4704s + 1} \tag{IV.2}$$

$$\frac{\Theta(s)}{F_i(s)} = G_{p12}(s) = \frac{-1.6e^{-546s}}{54.59s + 1} \tag{IV.3}$$

$$\frac{F_o(s)}{M(s)} = G_{p21}(s) = \frac{0.0012}{5964s + 1} \tag{IV.4}$$

$$\frac{\Theta(s)}{M(s)} = G_{p22}(s) = \frac{-0.063(1867s + 1)}{(801.06s + 1)(801.06s + 1)} \tag{IV.5}$$

where the *manipulated variables* are $F_i(s)$ that represents the inlet flow of material to mixer and $M(s)$ that represents the rotational velocity of the mixer, while the *controlled*

[1] CONTROL STATION ® FOR WINDOWS. Software Registered by Douglas J. Cooper.

variables are $F_o(s)$ that represents the material outlet flow from the mixer and $\Theta(s)$ that represents the variance of mixing.

From the principle of *superposition* and in vector-matrix notation, it follows that *simultaneous* changes in $F_i(s)$ and $M(s)$ have an additive effect on each controlled variable:

$$\begin{bmatrix} F_o(s) \\ \Theta(s) \end{bmatrix} = \begin{bmatrix} G_{p11}(s) & G_{p12}(s) \\ G_{p21}(s) & G_{p22}(s) \end{bmatrix} \begin{bmatrix} F_i(s) \\ M(s) \end{bmatrix} \tag{IV.6}$$

$$\begin{bmatrix} F_o(s) \\ \Theta(s) \end{bmatrix} = \begin{bmatrix} \dfrac{0.9908}{4704s+1} & \dfrac{-1.6e^{-546s}}{54.59s+1} \\ \dfrac{0.0012}{5964s+1} & \dfrac{-0.063(1867s+1)}{(801.06s+1)(801.06s+1)} \end{bmatrix} \begin{bmatrix} F_i(s) \\ M(s) \end{bmatrix} \tag{IV.7}$$

Eq. (IV.7) provides a compact representation in conventional control theory for the 2X2 *Multi Input Multi Output* (MIMO) system. Modern control theory is based on the description of the system's equations in terms of *n* first-order differential equations, which may be combined into a first-order vector-matrix differential equation which is essentially a time-domain approach. In the other hand, conventional control theory is a complex frequency-domain approach. In the *state-space* analysis exists three types of variables that are involved in the modeling of dynamic system: input, output and state variables. The state variables of a dynamic system are the variables making up the smallest set of variables that determine the state of the dynamic system [17]. The state-space representation for a system is not unique, except that the number of state variables is the same for any of the different state-space representations. Any set of transfer functions of any system can be represented in state-space by the following form:

$$\begin{aligned} \dot{\mathbf{x}}(t) &= \mathbf{A}\mathbf{x}(t) + \mathbf{B}\mathbf{u}(t) \\ \mathbf{y}(t) &= \mathbf{C}\mathbf{x}(t) + \mathbf{D}\mathbf{u}(t) \end{aligned} \tag{IV.8}$$

where **A** is called the state matrix, **B** the input matrix, **C** the output matrix, **D** the direct transmission matrix, $\mathbf{u}(t)$ the control vector, $\mathbf{x}(t)$ the state vector and $\mathbf{y}(t)$ the output vector.

A description of the conversion from compact representation in conventional control theory for the 2X2 MIMO system, Eq. (IV.7), to state-space representation in Matlab® is provided in Appendices B through E. The state, input, output and the direct transmission matrices are respectively:

$$\mathbf{A} = \begin{bmatrix} -0.0002 & 0 & 0 & 0 & 0 \\ 0 & -0.0002 & 0 & 0 & 0 \\ 0 & 0 & -0.0183 & 0 & 0 \\ 0 & 0 & 0 & -0.0025 & -0.0004 \\ 0 & 0 & 0 & 0.0039 & 0 \end{bmatrix} \tag{IV.9}$$

$$\mathbf{B} = \begin{bmatrix} 0.0156 & 0 \\ 0.0005 & 0 \\ 0 & 0.1250 \\ 0 & 0.0156 \\ 0 & 0 \end{bmatrix} \tag{IV.10}$$

$$\mathbf{C} = \begin{bmatrix} 0.0135 & 0 & -0.2345 & 0 & 0 \\ 0 & 0.0004 & 0 & -0.0117 & -0.0016 \end{bmatrix} \tag{IV.11}$$

$$\mathbf{D} = \begin{bmatrix} 0 & 0 \\ 0 & 0 \end{bmatrix} \tag{IV.12}$$

Then, the state-space representation of the rotated powder mixer is:

$$\dot{\mathbf{x}}(t)=\begin{bmatrix} -0.0002 & 0 & 0 & 0 & 0 \\ 0 & -0.0002 & 0 & 0 & 0 \\ 0 & 0 & -0.0183 & 0 & 0 \\ 0 & 0 & 0 & -0.0025 & -0.0004 \\ 0 & 0 & 0 & 0.0039 & 0 \end{bmatrix}\mathbf{x}(t)+\begin{bmatrix} 0.0156 & 0 \\ 0.0005 & 0 \\ 0 & 0.1250 \\ 0 & 0.0156 \\ 0 & 0 \end{bmatrix}\mathbf{u}(t)$$

$$\mathbf{y}(t)=\begin{bmatrix} 0.0135 & 0 & -0.2345 & 0 & 0 \\ 0 & 0.0004 & 0 & -0.0117 & -0.0016 \end{bmatrix}\mathbf{x}(t) \qquad \text{(IV.13)}$$

where:

$$\mathbf{u}(t)=\begin{bmatrix} F_i \\ M \end{bmatrix} \quad and \quad \mathbf{y}(t)=\begin{bmatrix} F_o \\ \Theta \end{bmatrix} \qquad \text{(IV.14)}$$

IV.3 **Model Validation**

The validation of the representations of the original model described by Eqs. (IV.7) and (IV.13) was performed in Simulink® (Matlab® tool) and plotted in Figure IV.1. The three models, time domain, transfer functions and state-space were ran in parallel with a simulation time of 60 000 seconds and subjected to the same changes in the inputs variables.

Computing the SSE between the response obtained by the model in time domain and both models in transfer functions and state-space according to Eq. (IV.1) the following values were obtained:

$$SSE^{Flow\_Out}_{Transfer\_Functions}=56146 \qquad SSE^{Flow\_Out}_{State-Space}=56563 \qquad \text{(IV.15)}$$

$$SSE^{Variance}_{Transfer\_Functions}=1.6397 \qquad SSE^{Variance}_{State-Space}=1.6578 \qquad \text{(IV.16)}$$

These results show that both models represent with the same trend and error level the time domain. However, the variance shows a better agreement than the outlet flow which has a higher non-linearity relation.

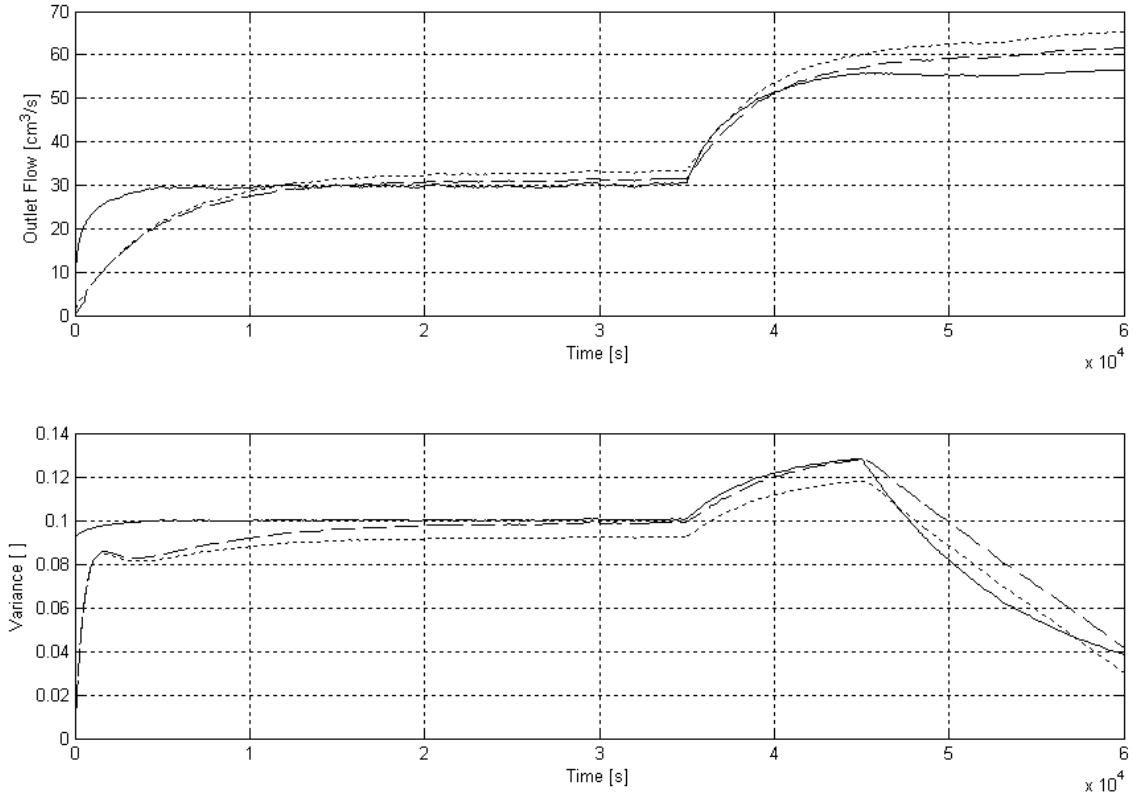

Figure IV.1 Response of the rotated mixer system. Model in time domain (solid), model in transfer functions (dashed), model in state-space (dotted).

IV.4 **Output controllability**

For the practical design of a control system, it is desired to control the output rather than the state of the system. Complete state controllability is neither necessary nor sufficient for controlling the output of the system. Considering the system described by Eq. (IV.8) where $\mathbf{x}$ the state vector has a size *n*, the control vector $\mathbf{u}$ has a size *r*, the output vector $\mathbf{y}$ has a size *m*, $\mathbf{A}$ is a matrix $n \times n$, $\mathbf{B}$ is a matrix $n \times r$, $\mathbf{C}$ is a matrix $m \times n$ and $\mathbf{D}$ is a matrix $m \times r$, it is said to be completely output controllable if and only if it is possible to construct an unconstrained control vector $\mathbf{u}(t)$ that will transfer any

given initial output $\mathbf{y}(t_0)$ to any final output $\mathbf{y}(t_1)$ in a finite time interval $t_0 \le t \le t_1$. Therefore, the system is completely output controllable if and only if the $m \times (n+1)r$ matrix

$$\left[\mathbf{CB} \mid \mathbf{CAB} \mid \mathbf{CA}^2\mathbf{B} \mid \ldots \mid \mathbf{CA}^{n-1}\mathbf{B} \mid \mathbf{D}\right]$$

is of rank m.

In this case study, the matrix $\mathbf{D}$ is equal to zero, m and r are equal to 2 and n is equal to 5. Then the system is completely output controllable if and only if the composite $m \times nr$ matrix **CON** defined as

$$\mathbf{CON} = \left[\mathbf{CB} \mid \mathbf{CAB} \mid \mathbf{CA}^2\mathbf{B} \mid \mathbf{CA}^3\mathbf{B} \mid \mathbf{CA}^4\mathbf{B}\right]$$

is of rank m. Computing the rank of matrix **CON** from Eqs. (IV.9) to (IV.11), it is obtained:

$$\mathbf{CON} = \begin{bmatrix} 0.0002 & -0.0293 & -0 & 0.0005 & 0 & -0 & -0 & 0 & 0 & -0 \\ 0 & -0.0002 & -0 & 0 & 0 & -0 & -0 & 0 & 0 & -0 \end{bmatrix} \quad \text{(IV.17)}$$

where the rank is equal to 2, proving that the system is completely output controllable.

IV.5 **Observability**

The system is said to be completely observable if every state $\mathbf{x}(t_0)$ can be determined from the observation of $\mathbf{y}(t)$ over a finite interval, $t_0 \le t \le t_1$. The system is, therefore, completely observable if every transition of the state eventually affects every element of the output vector. Mathematically, the system described by Eq. (IV.8) is completely observable if and only if the $n \times nm$ matrix

$$\left[\mathbf{C}^T \mid \mathbf{A}^T\mathbf{C}^T \mid \ldots \mid \left(\mathbf{A}^T\right)^{n-1}\mathbf{C}^T\right]$$

is of rank n or has n linearly independent column vectors. Similar to the controllability proof, the rank of the matrix **OBS** from Eqs. (IV.9) and (IV.11) is computing as

$$\mathbf{OBS} = \left[\mathbf{C}^T \mid \mathbf{A}^T\mathbf{C}^T \mid \left(\mathbf{A}^T\right)^2\mathbf{C}^T \mid \left(\mathbf{A}^T\right)^3\mathbf{C}^T \mid \left(\mathbf{A}^T\right)^4\mathbf{C}^T\right]$$

$$\mathbf{OBS} = \begin{bmatrix} 0.0135 & 0 & -0 & 0 & 0 & 0 & -0 & 0 & 0 & 0 \\ 0 & 0.0004 & 0 & -0 & 0 & 0 & 0 & -0 & 0 & 0 \\ -0.2345 & 0 & 0.0043 & 0 & -0.001 & 0 & 0 & 0 & -0 & 0 \\ 0 & -0.0117 & 0 & 0 & 0 & -0 & 0 & 0 & 0 & -0 \\ 0 & -0.0016 & 0 & 0 & 0 & -0 & 0 & 0 & 0 & -0 \end{bmatrix} \quad \text{(IV.18)}$$

where the rank is equal to 5, proving that the system is completely observable.

IV.6 **Multivariable control**

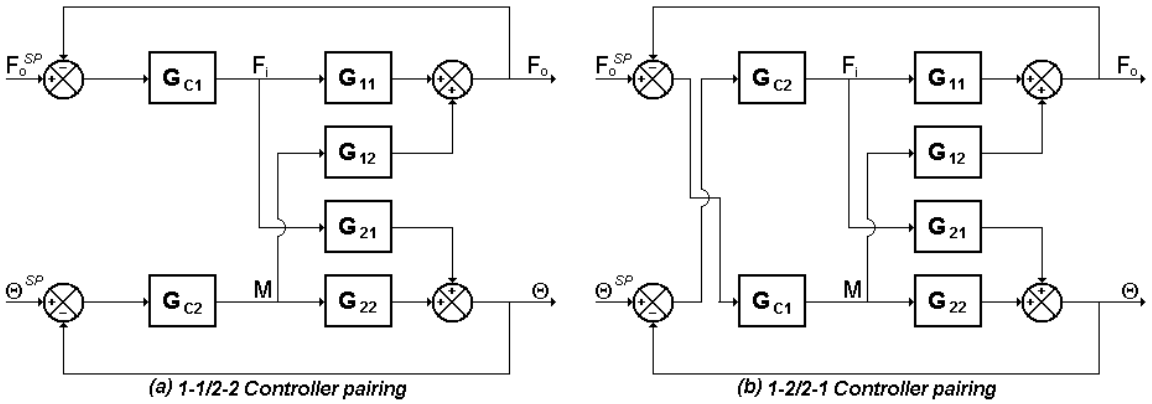

Figure IV.2 Controller pairing options for continuous tumble mixer.

Since the continuous tumble mixer in study is a MIMO system with two controlled variables and two manipulated variables, it is necessary to select the correct pairing of controlled and manipulated variables from the two options showed in Figure IV.2. A wrong pairing will result in poor control system performance and reduced

stability margins. Next, it is considered a systematic approach for determining the best pairing of controlled and manipulated variables, the *Relative Gain Array* (RGA) method.

IV.6.1 Pairing of controlled and manipulated variables

The pairing of variables is determined by the relative gain array:

$$\Lambda = \begin{bmatrix} \lambda_{11} & \lambda_{12} \\ \lambda_{21} & \lambda_{22} \end{bmatrix} \tag{IV.19}$$

where each element λ_{ij} between a controlled variable y_i and a manipulated variable u_j is determined by:

$$\lambda_{ij} \overset{\Delta}{=} \frac{\left(\partial y_i / \partial u_j\right)_u}{\left(\partial y_i / \partial u_j\right)_y} = \frac{open-loop \quad gain}{closed-loop \quad gain} \tag{IV.20}$$

In this work, the subscripts *i* and *j* take the values of either 1 or 2. The relative gain λ_{11} in Eq. (IV.19), for a 2X2 MIMO system is equal to:

$$\lambda_{11} = \frac{1}{1 - \dfrac{K_{12}K_{21}}{K_{11}K_{22}}} \tag{IV.21}$$

Because each row and each column of $\mathbf{\Lambda}$ in Eq. (IV.19) sums to one, the other relative gains are easily calculated from λ_{11} for the 2X2 case as:

$$\lambda_{12} = \lambda_{21} = 1 - \lambda_{11} \quad \text{and} \quad \lambda_{22} = \lambda_{11} \tag{IV.22}$$

thus, the RGA for the system can be expressed as:

$$\Lambda = \begin{bmatrix} \lambda & 1-\lambda \\ 1-\lambda & \lambda \end{bmatrix} \tag{IV.23}$$

The relative gains are easily calculated from the process model, represented by the Eq. (IV.7), where for a stable process:

$$\mathbf{K} = \mathbf{G_p}(0) = \lim_{s \to 0} \mathbf{G_p}(s) \tag{IV.24}$$

Therefore:

$$\mathbf{K} = \mathbf{G_P}(0) = \begin{bmatrix} 0.9908 & 0.0012 \\ -1.6 & -0.063 \end{bmatrix} \tag{IV.25}$$

and hence:

$$\Lambda = \begin{bmatrix} 1.0316 & -0.0316 \\ -0.0316 & 1.0316 \end{bmatrix} \tag{IV.26}$$

The positive relative gains and closer to one as possible establish the pairing of the controlled and manipulated variables. However, this method is based solely on steady-state information, ignoring the process dynamics, which can be an important factor in the pairing decision. If a paring of inputs and outputs corresponds to a negative relative gain, then the close-loop system will exhibit instability in the overall close-loop system. Thus, the RGA analysis indicates the 1-1/2-2 pairing should be used for the control design of the rotated mixer, this is, F_o should be controlled by F_i and Θ by M .

The RGA does not indicate severe interactions, therefore it is not necessary to use *decoupling control*. Decoupling improve control performance only when process interaction is unfavorable, so favorable interaction should not be reduced by decoupling. The stability and performance of full decoupling can be very sensitive to model error when the relative gain is greater than 1.

However, the ideal decoupling transfer functions for the continuous tumble mixer system would be:

$$T_{12}(s) = -\frac{G_{12}(s)}{G_{11}(s)} = \frac{7526s + 1.6}{54.09s + 0.9908} * e^{-546s} \qquad \text{(IV.27)}$$

$$T_{21}(s) = -\frac{G_{21}(s)}{G_{22}(s)} = \frac{770s^2 + 1.923s + 0.0012}{701500s^2 + 493.4s + 0.063} \qquad \text{(IV.28)}$$

The decoupler described by the Eq. (IV.27) is a *lead-lag unit* with dead time and it cancel the effect of variance output controller over $F_o(s)$, while the decoupler described by the Eq. (IV.28) is a dynamic model with two zeros and two poles, and it cancel the effect of outlet flow output controller over $\Theta(s)$, being both physically realizable, but not recommended by theirs dynamic characteristics, this is the high value of dead time and presence of zeros.

IV.6.2 Tuning of multiloop PI control system

Several methods have been proposed for estimating the tuning for multiloop systems without the time-consuming iterations associated with trial and error or the computer computations associated with the optimization approach [18]. Seborg *et al.* [5] present four types of tuning methods for multiloop PID control systems:

- Detuning method (Luyben, 1986)
- Sequential loop tuning method (Hovd and Skogestad, 1994)
- Independent loop method (Grosdidier and Morari, 1987; Skogestad and Morari, 1989)
- Relay auto-tuning (Shen and Yu, 1994)

An additional method bases the tuning on the characteristic equation for a 2X2 system, divided by $1 + G_{C2}(s)G_{11}(s)$ [18], which does not change the stability limit:

$$CE(s) = 1 + G_{C1}(s)G_{11}(s)\left(\frac{1 + G_{C2}(s)G_{22}(s)/\lambda_{11}(s)}{1 + G_{C2}(s)G_{22}(s)}\right) \quad \text{(IV.29)}$$

From the RGA analysis made for the continuous tumble mixer, it was established 1-1/2-2 pairing for the control design, that is $F_o(s) - F_i(s) / \Theta(s) - M(s)$. In Eq. (IV.7), it can be seen that the transfer function that relate $F_o(s) - F_i(s)$ is much slower than the transfer function that relate $\Theta(s) - M(s)$. When the first loop is much slower, the term for the fast controller would have a very large magnitude at the critical frequency of first loop, because the amplitude ratio of the integral mode in $G_{C2}(j\omega)$ will have a very high value at a frequency much less than the second loop critical frequency. Therefore, $|G_{C2}(j\omega)| >> 1$, which leads to the following simplification in the characteristic equation:

$$CE(j\omega) \approx 1 + G_{C1}(j\omega)G_{11}\left(\frac{G_{C2}(j\omega)G_{22}(j\omega)/\lambda_{11}}{G_{C2}(j\omega)G_{22}(j\omega)}\right) \quad \text{(IV.30)}$$

$$CE(j\omega) \approx G_{C1}(j\omega)\frac{G_{11}(j\omega)}{\lambda_{11}} \quad \text{(IV.31)}$$

Summarizing, the first loop stability is affected by the change in close-loop process gain, therefore the gain of single-loop controller must be divided by λ_{11}. Thus, for the first loop:

$$\frac{G_{p11}(s)}{\lambda_{11}} = \frac{0.9908 \diagup 1.0316}{4704s + 1} = \frac{0.9604}{4704s + 1} \quad \text{(IV.32)}$$

The *Internal Model Control* (IMC) method [19] was used to derive PI controller settings for the $F_o(s) - F_i(s)$ loop from the corresponding FOPDT transfer function:

$$\frac{K_P}{\tau s+1}=\frac{0.9604}{4704s+1} \tag{IV.33}$$

where:

$$K_C K_P=\frac{\tau}{\tau_c} \tag{IV.34}$$

$$\tau_I=\tau \tag{IV.35}$$

In Eq. (IV.34) τ_c is a design parameter. An increase of this parameter produces a more conservative controller because K_C decreases while τ_I increases. A good rule of thumb for selection of this parameter is 20% of the dominant time constant of the process model. From Eq. (IV.33):

$$\tau_c=\frac{\tau_{dom}}{5}=\frac{4704\,\text{sec}}{5}=940.8\,\text{sec} \tag{IV.36}$$

The value of $\tau_c=940.8$ means that the desired closed-loop response is five times faster than the open-loop response. Substituting the corresponding values into (IV.34) and (IV.35) it was obtained:

$$K_C^1=5.21 \tag{IV.37}$$

$$\tau_I^1=4704 \tag{IV.38}$$

For the second loop, the transfer function for the controller parameters is G_{p22}, described by Eq. (IV.5), which is a second order with lead time model. For this model, controller tuning values are not available in IMC relations, therefore, G_{p22} must be

approximated by a first order model. For this approximation, the model fitting tool of *Control Station Software* was used once again:

$$G_{p22}(s) = \frac{-0.063(1867s+1)}{(801.06s+1)(801.06s+1)} \approx \frac{-0.063}{53.4s+1} \qquad \text{(IV.39)}$$

The second order with lead time model, Eq. (IV.5), produced an $R^2 = 0.8823$ and a $SSE = 0.0062$, while the fist order model, Eq. (IV.39), produced an $R^2 = 0.8613$ and a $SSE = 0.0073$. Figure IV.2 depicts the response of both transfer functions to a step change in the input.

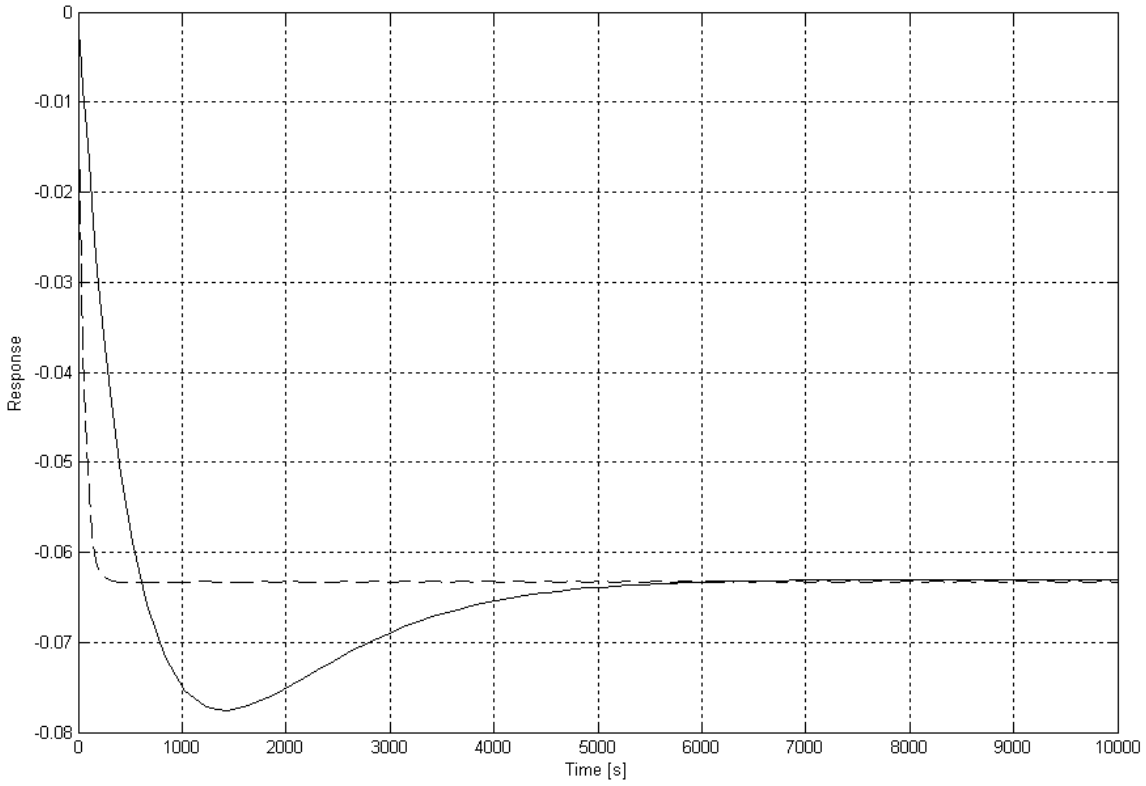

Figure IV.3 Response after a step change of G_{p22}. According to Eq. (IV.5) (solid), and according to approximation (IV.39) (dashed).

After the approximation and as the second loop is much faster than first loop, it is desired, as a design condition, that closed-loop response will be two times faster than the

open-loop response. Again, evaluating Eqs. (IV.34), (IV.35) and (IV.36) using Eq. (IV.39), the following values are obtained:

$$\tau_c = 53.4\,\text{sec} \big/ 2 = 26.7\,\text{sec} \tag{IV.40}$$

$$K_C^2 = \frac{53.4\,\text{sec}}{0.063 * 26.7\,\text{sec}} = 31.6 \tag{IV.41}$$

$$\tau_I^2 = 53.4 \tag{IV.42}$$

IV.6.3 Implementation of multiloop PI control system

Once the tuning parameters were determined, the close loop system was simulated in Simulink®, where the model in transfer functions were executed with a simulation time of 40 000 seconds with the following changes in the variables:

- Set-Point in Outlet Flow:

Table IV.1 Set-point change of outlet flow with PI controllers.

Time [sec]	Final Value [cm^3/s]	Change Type
0	5	---
4 000	40	Step
22 000	30	Step
40 000	30	---

- Load Disturbance (noise) over Outlet Flow:

Table IV.2 Load disturbance over outlet flow with PI controllers.

Time [sec]	Random [cm^3/s]	Change Type
0	0	---
9 000	+/- 1e-4	Frequency 50 sec
40 000	+/- 1e-4	Frequency 50 sec

- Set-Point in Variance:

Table IV.3 Set-point change of variance with PI controllers.

Time [sec]	Final Value [ ]	Change Type
0	0.04	---
6 000	0.03	Step
11 000	1e-6 sec^{-1}	Ramp
17 000	0.011	Step
40 000	0.011	---

- Load Disturbance (noise) over Variance:

Table IV.4 Load disturbance over variance with PI controllers.

Time [sec]	Random [ ]	Change Type
0	+/- 1e-9	Frequency 50 sec
17 000	0	---
40 000	0	---

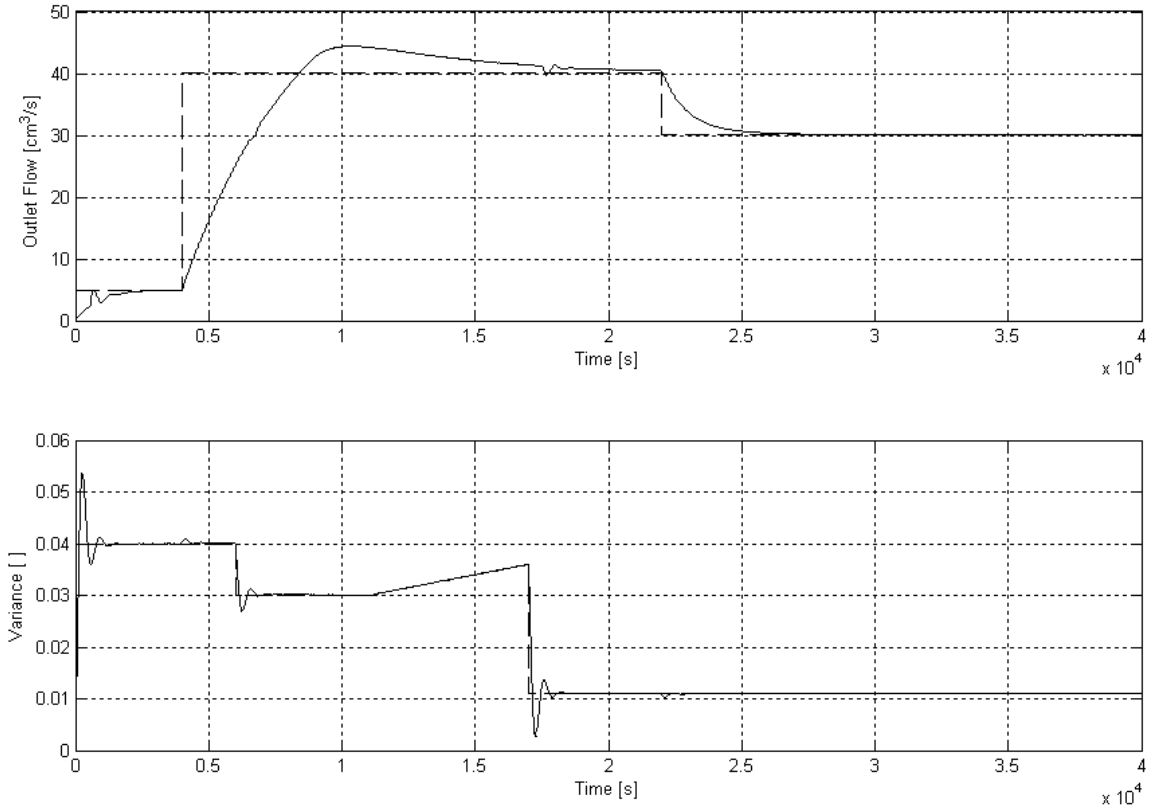

Figure IV.4 Multiloop PI control over model in Laplace domain. (a) Outlet Flow, (b) Variance. Set-Point (dashed), Variable (solid).

Figure IV.3 depicts the multiloop PI control over model process in Laplace domain for changes in set-points and disturbances. Figure IV.4 depicts the multiloop PI control too, but this time over time domain.

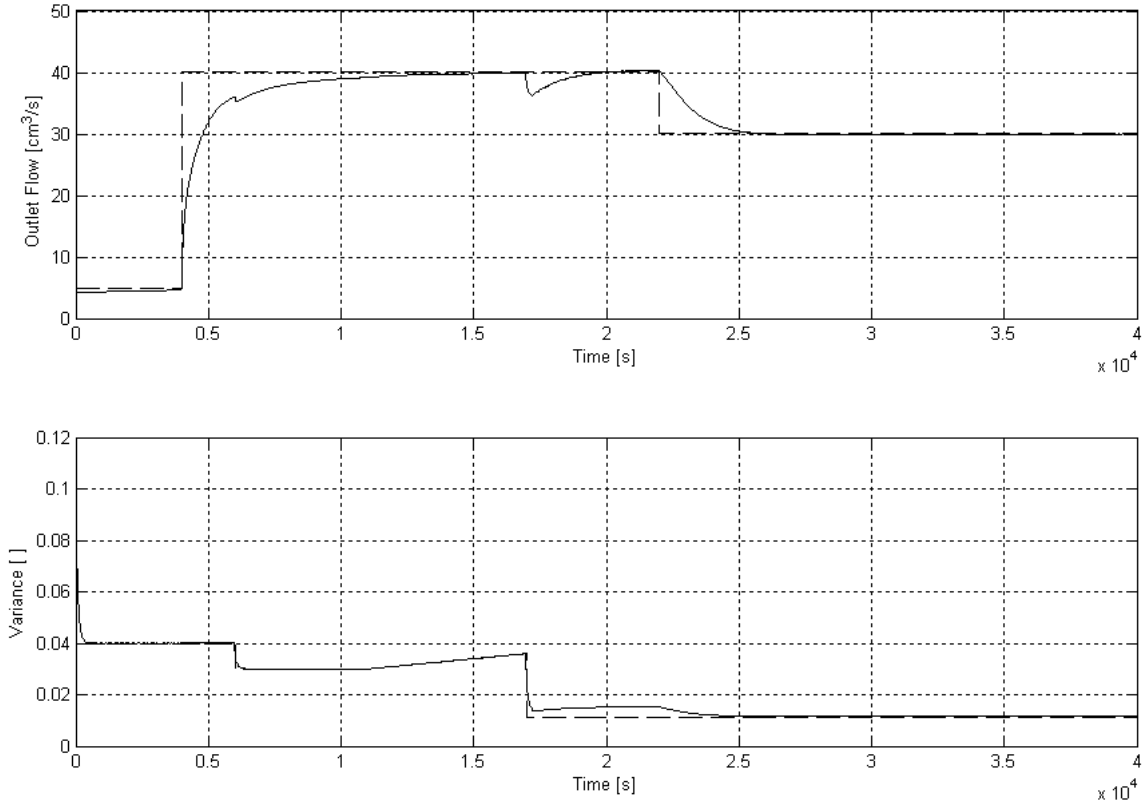

Figure IV.5 Multiloop PI control over model in time domain. (a) Outlet Flow, (b) Variance. Set-Point (dashed), Variable (solid).

In order to determine an appropriate operating point such that product quality may be guaranteed, the controller performance was tested with the combination of changes in set-points described above. The closed-loop performance in state-steady is reasonably well-controlled for both the Laplace domain and time domain, which confirm that the computation of tuning parameters for PI controllers from an approximate model is a good tool for initial tuning constants. The set-point tracking with the model in Laplace domain presents small overshoots, while with the model in time domain do not present. Both models do not present oscillations in the controlled variables and the interactions are

corrected without sacrificing stability. The disturbance rejection performance was very smooth and will be analyzed in chapter VI.

The trend of the manipulated variables with the model in time domain is shown in Figure IV.5. It can be seen tat they do not present large changes that could affect the behavior of the final elements. The constraints of the manipulated variables fixed in the simulations were: The inlet flow changed between 0 to 64 cm^3/s and the mixer velocity between 0 to 4 rps.

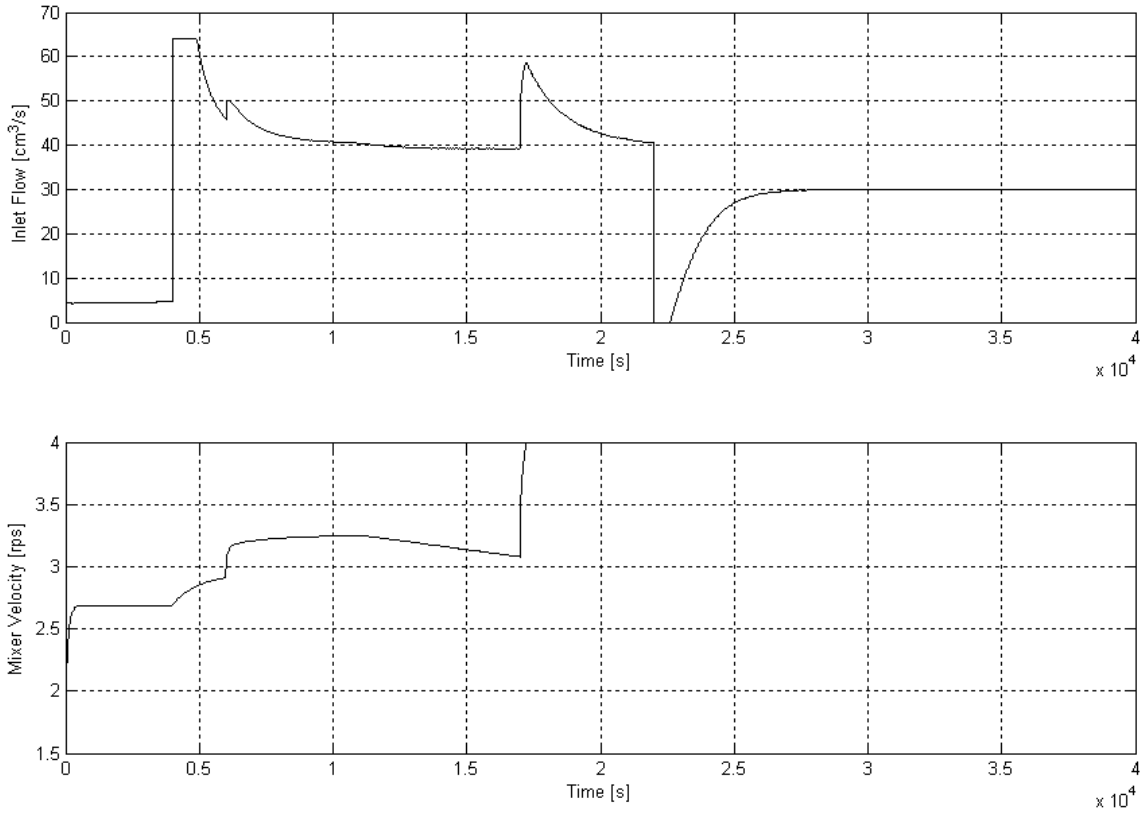

Figure IV.6 Multiloop PI control over model in time domain. (a) Inlet Flow, (b) Mixer Velocity.

CHAPTER V: MULTIVARIABLE CONTROL - MPC DESIGN

V.1 Goal of the multivariable MPC control

This chapter is focused on the design and analysis of a *Model Predictive Control* (MPC) strategy applied to the continuous tumble mixer in study. MPC [20,21] is an optimization based strategy that uses a plant model to predict the effect of potential control actions on the evolving state of the plant. At each time step, an open-loop optimal control problem is solved by a linear program (LP) or quadratic program (QP) and the input profile is injected into the plant until a new measurement becomes available.

To develop the strategy of described above, the *Model Predictive Control toolbox of Matlab*® will be used. This toolbox is a collection of software that helps to design, analyze and implement advanced industrial automation algorithms.

V.2 Overview of MPC for the continuous tumble mixer

An MPC strategy is a discrete-time controller; this is, it takes action at regularly-spaced, discrete time instants [22]. The sampling instants are the times at which the controller acts. The interval separating successive sampling instants is the *sampling period*, Δt.

The block diagram for model predictive control is provided in Appendix I, while Figure V.1 shows the state of a MPC system that has been operating for many sampling instants. Integer k represents the current instant. The latest measured outputs vector, $\mathbf{y}_k$, and previous measurements, $\mathbf{y}_{k-1}$, $\mathbf{y}_{k-2}$,…, are known. The previous moves vectors are represented by $\mathbf{u}_{k-4}$, …, $\mathbf{u}_{k-1}$. As is usually the case, a *zero-order hold array* receives each set of move from the controller and holds it until the next sampling instant, causing the step-wise variations.

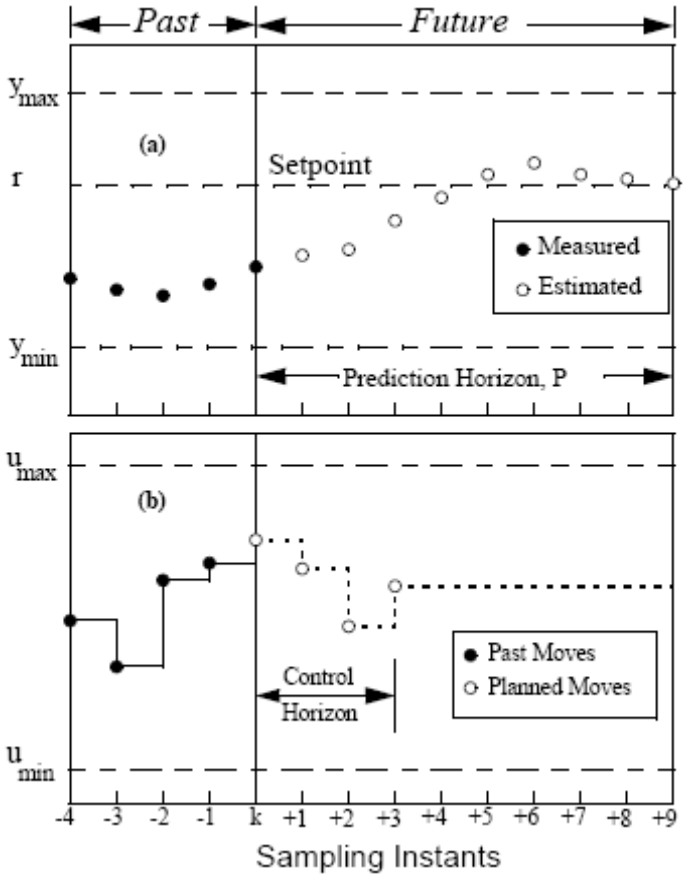

Figure V.1 Basic concept for MPC [22].

To calculate its next move $\mathbf{u}_k$, the controller operates in two phases [22]:

V.2.1 Estimation

In order to make an optimum controller move, the controller needs to know the current state. This includes the true value of the controlled variable set $\bar{\mathbf{y}}_k$, and any interval variables that influence the future trend, $\bar{\mathbf{y}}_{k+1}$, …, $\bar{\mathbf{y}}_{k+P}$.

V.2.2 Optimization

Values of set-points, measured disturbances, and constraints are specified over a finite *horizon* of future sampling instants, $k+1$, $k+2$, …, $k+P$, where P is the

prediction horizon. The controller computes *M* moves $\mathbf{u}_k$, $\mathbf{u}_{k+1}$, …, $\mathbf{u}_{k+M-1}$, where *M* is the *control horizon*. Some typical rules of thumb to select *M* [5] are $5 \le M \le 20$ and $N/3 < M < N/2$, where:

$$N = \frac{t_s}{\Delta t} \tag{V.1}$$

t_s is the settling time for the open-loop response. For the present research, $N = 35$, $\Delta t = 1$ and $M = 15$, fulfilling with the rules specified above. The prediction horizon *P* is often selected to be $P = N + M$, this is $P = 50$.

V.3 **Prediction and optimization model**

The linear model used in the design of MPC for prediction and optimization is depicted in Figure V.2.

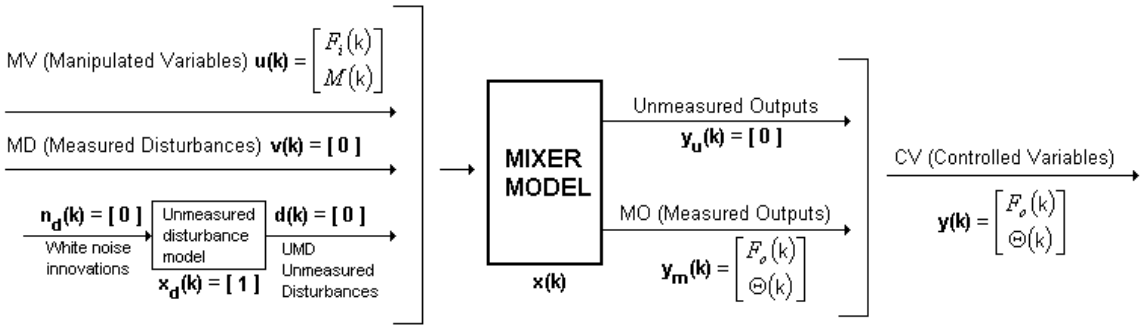

Figure V.2 Linear model for MPC for a continuous tumble mixer.

In the Matlab MPC toolbox of [22], the model of the plant is a linear time-invariant system described by the equations:

$$\mathbf{x}(k+1) = \mathbf{A}\mathbf{x}(k) + \mathbf{B}_u\mathbf{u}(k) + \mathbf{B}_v\mathbf{v}(k) + \mathbf{B}_d\mathbf{d}(k) \tag{V.2}$$

$$\mathbf{y}_m(k) = \mathbf{C}_m\mathbf{x}(k) + \mathbf{D}_{vm}\mathbf{v}(k) + \mathbf{D}_{dm}\mathbf{d}(k) \tag{V.3}$$

$$\mathbf{y}_u(k) = \mathbf{C}_u \mathbf{x}(k) + \mathbf{D}_{vu}\mathbf{v}(k) + \mathbf{D}_{du}\mathbf{d}(k) + \mathbf{D}_{uu}\mathbf{u}(k) \tag{V.4}$$

where $\mathbf{x}(k)$ is the n_x-dimensional state vector of the plant, $\mathbf{u}(k)$ is the n_u-dimensional vector of manipulated variables, $\mathbf{v}(k)$ is the n_v-dimensional vector of measured disturbances, $\mathbf{d}(k)$ is the n_d-dimensional vector of unmeasured disturbances entering the plant, $\mathbf{y}_m(k)$ is the vector of measured outputs, and $\mathbf{y}_u(k)$ is the vector of unmeasured outputs. The matrices $\mathbf{A}, \mathbf{B}, \mathbf{C}, \mathbf{D}$ of the model that represent the continuous tumble mixer are defined by the Eqs. (IV.9) to (IV.12). The unmeasured disturbances $\mathbf{d}(k)$ is modeled as the output of the linear time invariant system:

$$\mathbf{x}_d(k+1) = \overline{\mathbf{A}}\mathbf{x}_d(k) + \overline{\mathbf{B}}\mathbf{n}_d(k) \tag{V.5}$$

$$\mathbf{d}(k) = \overline{\mathbf{C}}\mathbf{x}_d(k) + \overline{\mathbf{D}}\mathbf{n}_d(k) \tag{V.6}$$

The system described by the above equations is driven by the random Gaussian noise $\mathbf{n}_d(k)$, having zero mean and unit covariance matrix.

The MPC control action at time k is obtained by solving the optimization problem [22]:

$$\Delta\mathbf{u}(k \mid k),\ldots,\Delta\mathbf{u}(M-1+k \mid k) = \overset{\min}{\varepsilon}\left\{ \sum_{i=0}^{P-1} \left(\begin{array}{c} \sum_{j=1}^{N_\mathbf{y}} \left| \mathbf{w}^{\mathbf{y}}_{i+1,j} \left(\mathbf{y}_j(k+i+1 \mid k) - \mathbf{r}_j(k+i+1) \right) \right|^2 \\ + \sum_{j=1}^{N_\mathbf{u}} \left| \mathbf{w}^{\Delta\mathbf{u}}_{i,j} \Delta\mathbf{u}_j(k+i \mid k) \right|^2 \\ + \sum_{j=1}^{N_\mathbf{u}} \left| \mathbf{w}^{\mathbf{u}}_{i,j} \left(\mathbf{u}_j(k+i \mid k) - \mathbf{u}_{j_{\text{target}}}(k+i) \right) \right|^2 \end{array} \right) + \rho_\varepsilon \varepsilon^2 \right\} \tag{V.7}$$

where the subscript $_j$ denotes the *j-th* component of a vector, "$(k+i\,|\,k)$" denotes the value predicted for time $k+i$ based on the information available at time k; $\mathbf{r}(k)$ is the current sample of the output reference, subject to:

$$\begin{aligned}
\mathbf{u}_{j\min}(i)-\varepsilon\mathbf{V}^{\mathbf{u}}_{j\min}(i)\le\mathbf{u}_j(k+i\,|\,k)\le\mathbf{u}_{j\max}(i)+\varepsilon\mathbf{V}^{\mathbf{u}}_{j\max}(i)\\
\Delta\mathbf{u}_{j\min}(i)-\varepsilon\mathbf{V}^{\Delta\mathbf{u}}_{j\min}(i)\le\Delta\mathbf{u}_j(k+i\,|\,k)\le\Delta\mathbf{u}_{j\max}(i)+\varepsilon\mathbf{V}^{\Delta\mathbf{u}}_{j\max}(i)\\
\mathbf{y}_{j\min}(i)-\varepsilon\mathbf{V}^{\mathbf{y}}_{j\min}(i)\le\mathbf{y}_j(k+i+1\,|\,k)\le\mathbf{y}_{j\max}(i)+\varepsilon\mathbf{V}^{\mathbf{y}}_{j\max}(i)\quad i=0,...,P-1\\
\Delta\mathbf{u}(k+h\,|\,k)=0, h=M,...P-1\\
\varepsilon\ge 0
\end{aligned}\tag{V.8}$$

with respect to the sequence of input increment $\{\Delta\mathbf{u}(k\,|\,k),...,\Delta\mathbf{u}(M-1+k\,|\,k)\}$ and to the slack variable ε, and by setting $\mathbf{u}(k)=\mathbf{u}(k-1)+\Delta\mathbf{u}(k\,|\,k)^*$, where $\Delta\mathbf{u}(k\,|\,k)^*$ is the first element of the optimal sequence. $\mathbf{w}^{\Delta\mathbf{u}}_{i,j}$, $\mathbf{w}^{\mathbf{u}}_{i,j}$, $\mathbf{w}^{\mathbf{y}}_{i,j}$, are nonnegative weight vectors for the corresponding set variables. The smaller w, the less important is the behavior of the corresponding variable to the overall performance index. $\mathbf{u}_{j,\min}$, $\mathbf{u}_{j,\max}$, $\Delta\mathbf{u}_{j,\min}$, $\Delta\mathbf{u}_{j,\max}$, $\mathbf{y}_{j,\min}$, $\mathbf{y}_{j,\max}$ are lower and upper bounds on the corresponding variables, commonly named as *constraints by bounds*. In equation (V.8), the constrains are relaxed by introducing the slack variable $\varepsilon\ge 0$. The weight ρ_ε on the slack variable ε penalizes de violation of the constraints. The Equal Concern for the Relaxation *ECR* vectors $\mathbf{V}^{\mathbf{u}}_{\min}$, $\mathbf{V}^{\mathbf{u}}_{\max}$, $\mathbf{V}^{\Delta\mathbf{u}}_{\min}$, $\mathbf{V}^{\Delta\mathbf{u}}_{\max}$, $\mathbf{V}^{\mathbf{y}}_{\min}$ y $\mathbf{V}^{\mathbf{y}}_{\max}$ have nonnegative entries which represent the concern for relaxing the corresponding constraint.

For our continuous tumble mixer, the values of measured outputs and controlled variables vectors in (V.2) to (V.8) are:

$$\mathbf{y}(k)=\mathbf{y}_m(k)=\begin{bmatrix}F_o(k)\\ \Theta(k)\end{bmatrix}\tag{V.9}$$

The manipulated variable vector is represented by:

$$\mathbf{u}(k) = \begin{bmatrix} F_i(k) \\ M(k) \end{bmatrix} \tag{V.10}$$

The disturbance model in Eqs. (V.5) and (V.6) is a unit gain, this is $\mathbf{d}(k) = \mathbf{n}_d(k)$ corresponding to a white Gaussian noise. Unmeasured outputs and measured disturbances vectors are zero, similarly to unmeasured disturbances and white noise innovations vectors:

$$\mathbf{v}(k) = \mathbf{d}(k) = \mathbf{n}_d(k) = \mathbf{y}_u(k) = [\mathbf{0}] \tag{V.11}$$

$$\mathbf{x}_d(k) = [\mathbf{1}] \tag{V.12}$$

The constraints are divided in two types: hard and soft. Hard constraints are those that can not be violated, and if necessary, the controller ignores its other objectives in order to satisfy them, for this may cause infeasibility of the optimization problem. Soft constraints can be violated with a fixed tolerance. In practical, lower and upper bounds, and maximum down and up rates of manipulated variables are hard constraints, since they are limits imposed by the final control elements of the system. As in previous chapter, the inlet flow changed between 0 to 64 cm^3/s and the mixer velocity between 0 to 4 rps. The maximum amount that the manipulated variables can decrease or increase in one move is unlimited. Therefore,

$$\mathbf{u}_{j,\min} = \begin{bmatrix} F_i \\ M \end{bmatrix}_{\min} = \begin{bmatrix} 0 \\ 0 \end{bmatrix} \tag{V.13}$$

$$\mathbf{u}_{j,\max} = \begin{bmatrix} F_i \\ M \end{bmatrix}_{\max} = \begin{bmatrix} 64 \\ 4 \end{bmatrix} \tag{V.14}$$

$$\Delta \mathbf{u}_{j,\min} = \begin{bmatrix} -\infty \\ -\infty \end{bmatrix} \tag{V.15}$$

$$\Delta \mathbf{u}_{j,\max} = \begin{bmatrix} \infty \\ \infty \end{bmatrix} \tag{V.16}$$

Constraints on maximum value of output variables are not defined in this study, because its definition will avoid the comparison with PI strategy implemented in previous chapter, however this is an important and useful parameter in design of MPC controller. Thus:

$$\mathbf{y}_{j,\min} = \begin{bmatrix} 0 \\ 0 \end{bmatrix} \tag{V.17}$$

$$\mathbf{y}_{j,\max} = \begin{bmatrix} \infty \\ \infty \end{bmatrix} \tag{V.18}$$

In Eq. (V.8), the *Equal Concern for the Relaxation* (ECR) vectors that multiply hard constraints have a zero value, while those that multiply soft constraints are equal to one, this is:

$$\mathbf{V}^{\mathbf{u}}_{\min} = \mathbf{V}^{\mathbf{u}}_{\max} = \mathbf{V}^{\Delta \mathbf{u}}_{\min} = \mathbf{V}^{\Delta u}_{\max} = [\mathbf{0}] \tag{V.19}$$

$$\mathbf{V}^{\mathbf{y}}_{\min} = \mathbf{V}^{\mathbf{y}}_{\max} = [\mathbf{1}] \tag{V.20}$$

Input and output weight vectors have strong influence over controller performance. On inputs, weight vector penalizes deviations of a manipulated variable from its nominal value, while outputs vector penalizes deviation from its set-point. When w values of a weight input vector or weight change input vector are zero, the manipulated variable can move between its upper and lower bound, while if the values are positives, this increases the weight to keep the manipulated variable near its nominal

value. A zero value of w into a weight output vector is used when the output does not have a set-point and a positive value increase the weight to keep the output close to its set-point. The model for the variance of mixing $\Theta(k)$ is a nonlinear output variable, due to its exponential behavior. In order to give priority to the function of mixing control, its w value in the weight output vector is very much higher than that of the $F_o(k)$. Weight input and weight change input vectors are set to zero, thus:

$$\mathbf{w}_{i,j}^{\mathbf{u}} = \mathbf{w}_{i,j}^{\Delta\mathbf{u}} = [\mathbf{0}] \tag{V.21}$$

$$\mathbf{w}_{i,j}^{\mathbf{y}} = \begin{bmatrix} 0.03 \\ 100 \end{bmatrix} \tag{V.22}$$

Finally, the value of the weight ρ_ε on the slack variable ε is by default [22]:

$$\rho_\varepsilon = 10^5 \max\left\{\mathbf{w}_{i,j}^{\Delta\mathbf{u}} \quad \mathbf{w}_{i,j}^{\mathbf{u}} \quad \mathbf{w}_{i,j}^{\mathbf{y}}\right\} \tag{V.23}$$

As the algorithm implemented in the toolbox of Matlab for the control of the continuous tumble mixer includes constraints, the solution of Eqs. (V.7) and (V.8) is obtained by a *Quadratic Programming* (QP) [22].

V.4 **QP matrices**

In the process to obtain the matrices associated with the MPC optimization problem, Bemporad *et al*. [22, 23] assume first, for the prediction, that the disturbance model in Eqs. (V.5) and (V.6) is a unit gain denoted by:

$$\mathbf{x} \leftarrow \begin{bmatrix} \mathbf{x} \\ \mathbf{x}_d \end{bmatrix}, \mathbf{A} \leftarrow \begin{bmatrix} \mathbf{A} & \mathbf{B}_d\overline{\mathbf{C}} \\ \mathbf{0} & \overline{\mathbf{A}} \end{bmatrix}, \mathbf{B}_u \leftarrow \begin{bmatrix} \mathbf{B}_u \\ \mathbf{0} \end{bmatrix}, \mathbf{B}_v \leftarrow \begin{bmatrix} \mathbf{B}_v \\ \mathbf{0} \end{bmatrix}, \mathbf{B}_d \leftarrow \begin{bmatrix} \mathbf{B}_d\overline{\mathbf{D}} \\ \overline{\mathbf{B}} \end{bmatrix}, \mathbf{C} \leftarrow \begin{bmatrix} \mathbf{C} & \mathbf{D}_d & \overline{\mathbf{C}} \end{bmatrix}$$

then, the prediction model is given now by:

$$\mathbf{x}(k+1) = \mathbf{A}\mathbf{x}(k) + \mathbf{B}_u\mathbf{u}(k) + \mathbf{B}_v\mathbf{v}(k) + \mathbf{B}_d\mathbf{n}_d(k) \tag{V.24}$$

$$\mathbf{y}(k) = \mathbf{C}\mathbf{x}(k) + \mathbf{D}_v\mathbf{v}(k) + \mathbf{D}_d\mathbf{n}_d(k) \tag{V.25}$$

The prediction of the future trajectories of the model performed at time $k = 0$ and $\mathbf{n}_d(i) = [\mathbf{0}]$ for all predictions instants *i*, and it is obtained [22]:

$$\mathbf{y}(i \mid 0) = \mathbf{C}\left[\mathbf{A}^i\mathbf{x}(0) + \sum_{h=0}^{i-1}\left(\mathbf{A}^{i-1}\mathbf{B}_u\left(\mathbf{u}(-1) + \sum_{j=0}^{h}\Delta\mathbf{u}(j)\right) + \mathbf{B}_v\mathbf{v}(h)\right)\right] + \mathbf{D}_v\mathbf{v}(i) \tag{V.26}$$

which gives

$$\begin{bmatrix} y(1) \\ \dots \\ y(P) \end{bmatrix} = \mathbf{S}_x\mathbf{x}(0) + \mathbf{S}_{u1}\mathbf{u}(-1) + \mathbf{S}_u\begin{bmatrix} \Delta u(0) \\ \dots \\ \Delta u(P-1) \end{bmatrix} + \mathbf{H}_v\begin{bmatrix} v(0) \\ \dots \\ v(P) \end{bmatrix} \tag{V.27}$$

where

$$\mathbf{S}_x = \begin{bmatrix} \mathbf{CA} \\ \mathbf{CA}^2 \\ \dots \\ \mathbf{CA}^P \end{bmatrix} \in \Re^{PN_{\mathbf{y}} \times N_{\mathbf{x}}} \tag{V.28}$$

$$\mathbf{S}_{u1} = \begin{bmatrix} \mathbf{CB}_u \\ \mathbf{CB}_u + \mathbf{CAB}_u \\ \dots \\ \sum_{h=0}^{P-1}\mathbf{CA}^h\mathbf{B}_u \end{bmatrix} \in \Re^{PN_{\mathbf{y}} \times N_{\mathbf{u}}} \tag{V.29}$$

$$\mathbf{S}_u = \begin{bmatrix} \mathbf{CB}_u & 0 & \dots & 0 \\ \mathbf{CB}_u + \mathbf{CAB}_u & \mathbf{CB}_u & \dots & 0 \\ \dots & \dots & \dots & \dots \\ \sum_{h=0}^{P-1} \mathbf{CA}^h \mathbf{B}_u & \sum_{h=0}^{P-2} \mathbf{CA}^h \mathbf{B}_u & \dots & \mathbf{CB}_u \end{bmatrix} \in \Re^{PN_\mathbf{y} \times PN_\mathbf{u}} \tag{V.30}$$

$$\mathbf{H}_v = \begin{bmatrix} \mathbf{CB}_v & \mathbf{D}_v & 0 & \dots & 0 \\ \mathbf{CAB}_v & \mathbf{CB}_v & \mathbf{D}_v & \dots & 0 \\ \dots & \dots & \dots & \dots & \dots \\ \mathbf{CA}^{P-1}\mathbf{B}_v & \mathbf{CA}^{P-2}\mathbf{B}_v & \mathbf{CA}^{P-3}\mathbf{B}_v & \dots & \mathbf{D}_v \end{bmatrix} \in \Re^{PN_\mathbf{y} \times (P+1)N_\mathbf{v}} \tag{V.31}$$

The optimization variables are calculated by the following algorithm [22]:

$$\begin{bmatrix} \Delta\mathbf{u}(0) \\ \dots \\ \Delta\mathbf{u}(P-1) \end{bmatrix} = \mathbf{J}_M \begin{bmatrix} \mathbf{z}_0 \\ \dots \\ \mathbf{z}_{M-1} \end{bmatrix} \tag{V.32}$$

where $\mathbf{J}_M$ depends on the choice of blocking moves. Together with the slack variable ε, vectors $\mathbf{z}_0$, …, $\mathbf{z}_{M-1}$ constitute the free optimization variables of the optimization problem. The function to be optimized is:

$$\mathbf{J}(z,\varepsilon) = \rho_\varepsilon \varepsilon^2 + \mathbf{z}^T \mathbf{K}_{\Delta\mathbf{u}} \mathbf{z} + 2 \left(\begin{bmatrix} \mathbf{r}(1) \\ \dots \\ \mathbf{r}(P) \end{bmatrix}^T \mathbf{K}_r + \begin{bmatrix} \mathbf{v}(0) \\ \dots \\ \mathbf{v}(P) \end{bmatrix} \mathbf{K}_v + \mathbf{u}(-1)^T \mathbf{K}_u + \begin{bmatrix} \mathbf{u}_{target}(0) \\ \dots \\ \mathbf{u}_{target}(P-1) \end{bmatrix} \mathbf{K}_{ut} + \mathbf{x}(0)^T \mathbf{K}_x \right) \mathbf{z} + G \tag{V.33}$$

where G is a constant and $\mathbf{K}$ are Hessian matrices. The constraints are involved through:

$$\mathbf{M}_z\mathbf{z} + \mathbf{M}_\varepsilon\varepsilon \le \mathbf{M}_{\lim} + \mathbf{M}_v\begin{bmatrix}\mathbf{v}(0)\\ \dots \\ \mathbf{v}(P)\end{bmatrix} + \mathbf{M}_u\mathbf{u}(-1) + \mathbf{M}_x\mathbf{x}(0) \qquad \text{(V.34)}$$

where matrices $\mathbf{M}_z$, $\mathbf{M}_\varepsilon$, $\mathbf{M}_{\lim}$, $\mathbf{M}_v$, $\mathbf{M}_u$ and $\mathbf{M}_x$ are obtained from the upper and lower bounds and ECR values [22]. The optimal solution $\mathbf{z}^*$, ε^* is computed by solving the quadratic program described in Eqs. (V.33) and (V.34).

V.5 **Implementation of MPC control**

The closed loop system with MPC controller was simulated in Simulink® with a simulation time of 40 000 seconds with the following changes in the variables:

- Set-Point in Outlet Flow:

Table V.1 Set-point change of outlet flow with MPC controller.

Time [sec]	**Final Value [cm^3/s]**	**Change Type**
0	40	---
10 000	50	Step
22 000	30	Step
36 000	-0.004 sec^{-1}	Ramp
40 000	14	---

- Load Disturbance (noise) over Outlet Flow:

Table V.2 Load disturbance over flow out with MPC controller.

Time [sec]	**Random [cm^3/s]**	**Change Type**
0	0	---
9 000	+/- 1e-4	Frequency 200 sec
40 000	+/- 1e-4	Frequency 200 sec

- Set-Point in Variance:

Table V.3 Set-point change of variance with MPC controller.

Time [sec]	Final Value [ ]	Change Type
0	0.04	---
6 000	0.03	Step
11 000	1e-6 sec^{-1}	Ramp
17 000	0.011	Step
40 000	0.011	---

- Load Disturbance (noise) over Variance:

Table V.4 Load disturbance over variance with MPC controller.

Time [sec]	Random [ ]	Change Type
0	+/- 1e-9	Frequency 200 sec
17 000	0	---
40 000	0	---

Figures V.3, V.4 and V.5 depict the MPC controller performance for the continuous tumble mixer, for the same changes in set-points and disturbances. The difference between the three figures is the value set for the output weight vectors $\mathbf{w}^{\mathbf{y}}_{i,j}$. Figure V.3 was obtained with $\mathbf{w}^{\mathbf{y}}_{i,j} = col[0.03,1]$, Figure V.4 with $\mathbf{w}^{\mathbf{y}}_{i,j} = col[0.03,10]$ and Figure V.5 with $\mathbf{w}^{\mathbf{y}}_{i,j} = col[0.03,100]$.

The results show that as w increases for the variance of mixing $\Theta(k)$ in the weight output vector, its value is closer to the set-point, while for $F_o(k)$ a light positive value of w keeps the output over its set-point. Large w values for any output variable keeps the output close to its set-point, with a possible sacrifice in stability for the others. This is observed as w in the variance is increased for the three figures, and w for $F_o(k)$ is maintained constant, starts showing light overshoots.

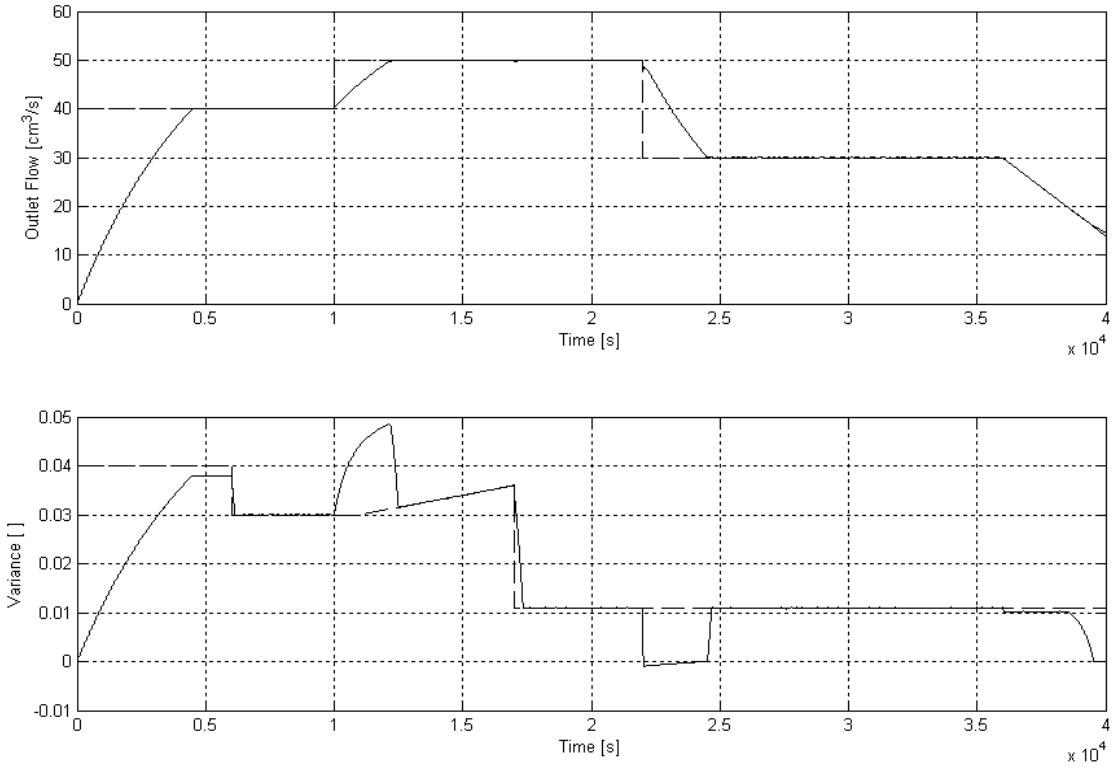

Figure V.3 MPC controller over continuous tumble mixer with $\mathbf{w}^{y}_{i,j}$ = col [0.03,1]. (a) Outlet Flow, (b) Variance. Set-Point (dashed), Variable (solid).

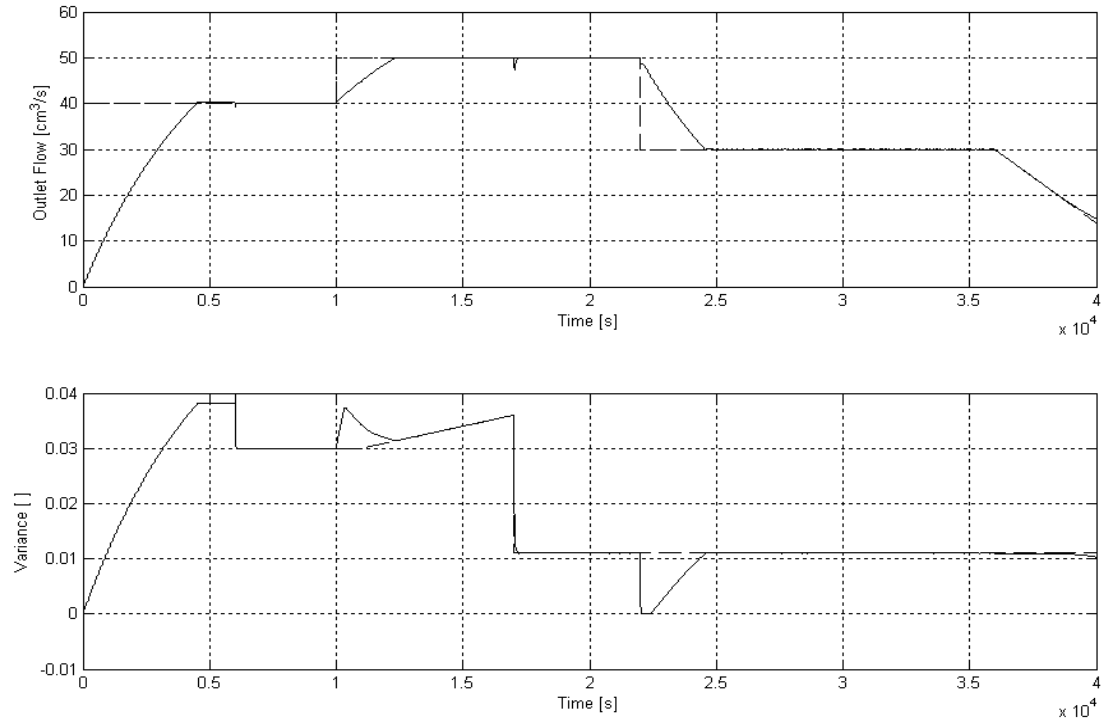

Figure V.4 MPC controller over continuous tumble mixer with $\mathbf{w}^{y}_{i,j}$ = col [0.03,10]. (a) Outlet Flow, (b) Variance. Set-Point (dashed), Variable (solid).

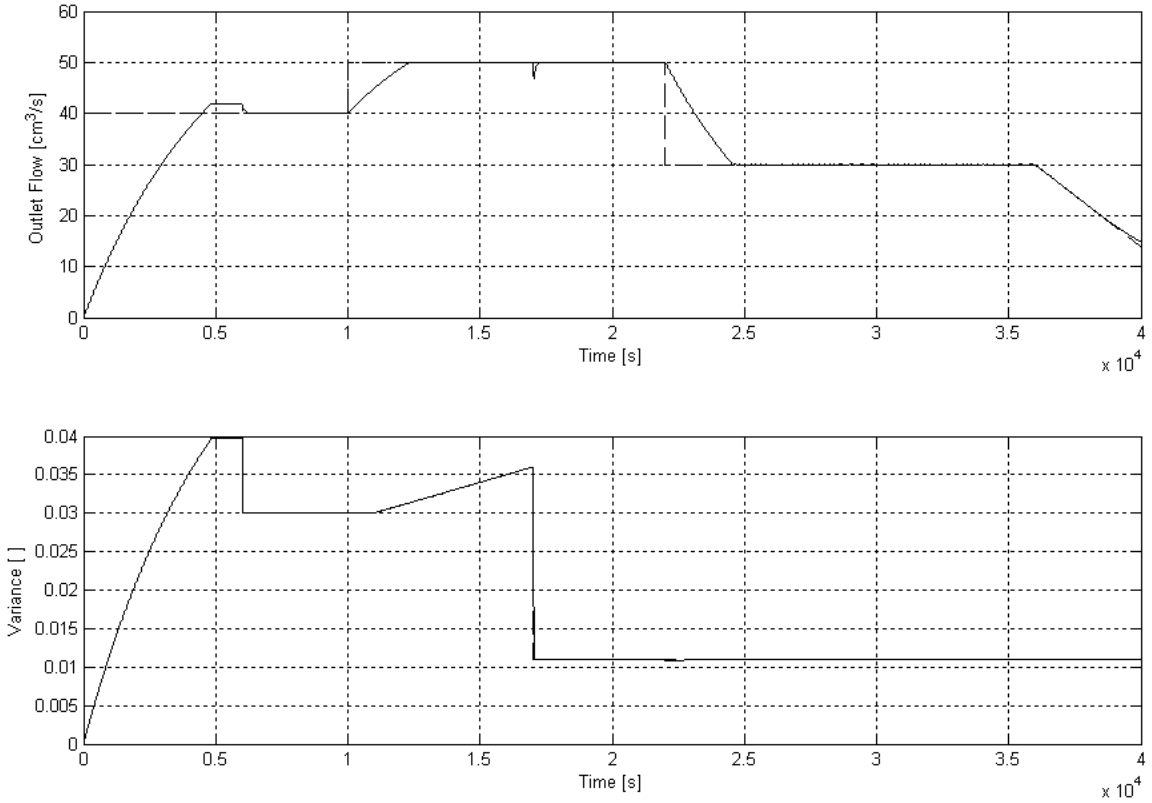

Figure V.5 MPC controller over continuous tumble mixer with $\mathbf{w}^{\mathbf{y}}_{i,j}$ = col [0.03,100]. (a) Outlet Flow, (b) Variance. Set-Point (dashed), Variable (solid).

With all values of $\mathbf{w}^{\mathbf{y}}_{i,j}$ the feedback system for MPC controller is stable, but with $\mathbf{w}^{\mathbf{y}}_{i,j} = col[0.03,100]$ the control over the variance of mixing $\Theta(k)$ is better for set-points tracking without present overshoots. The trend of manipulated variables is shown in Figure V.6 and it can be seen how they present some strong changes when the set-points tracking were registered by the controller.

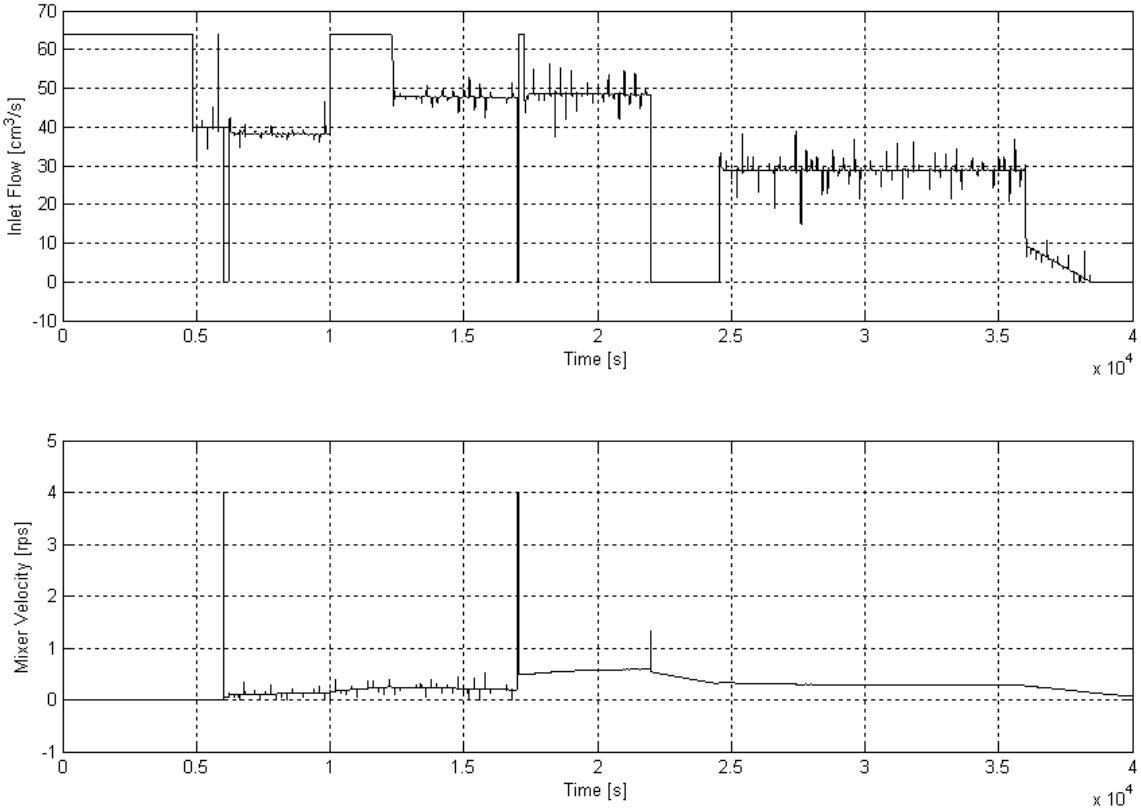

Figure V.6 MPC controller with $\mathbf{w}^{y}_{i,j}$ = col [0.03,100]. (a) Inlet Flow, (b) Mixer Velocity.

CHAPTER VI: MULTIVARIABLE CONTROL - MPC VERSUS PI

VI.1 Goal of the comparison

This chapter is focused on comparing the behavior and performance of two feedback PI controllers developed in chapter IV and that of the MPC strategy developed in chapter V, studying the stability, overshoots on set-point tracking, accurate ranges and capacity to reject the effect of load disturbances.

For the analysis, set-point changes and load disturbances were implemented over system for the analysis the proposed control strategies with step, ramp, sine wave and random changes, and the interaction effects between variables.

VI.2 Set-point tracking

The closed-loop system behavior for set-point changes is commonly referred as *servo problem*. While the set-point of a manipulated variable was maintained constant, set-point of the other manipulated variable was changed to study the performance of the controllers.

VI.2.1 Set-point changes in F_o

Figure VI.1 depicts the closed-loop response to set-point changes. For two step changes in F_o from 40 cm^3/s to 30 cm^3/s and 30 cm^3/s to 45 cm^3/s both controllers avoid overshoot and oscillations, but MPC controller is faster than outlet flow PI controller. These step changes generate overshoots over Θ, but MPC controller does not presents oscillations to reestablish the process variable to its set point, while with variance PI controller the decay ratio is 20% approximately.

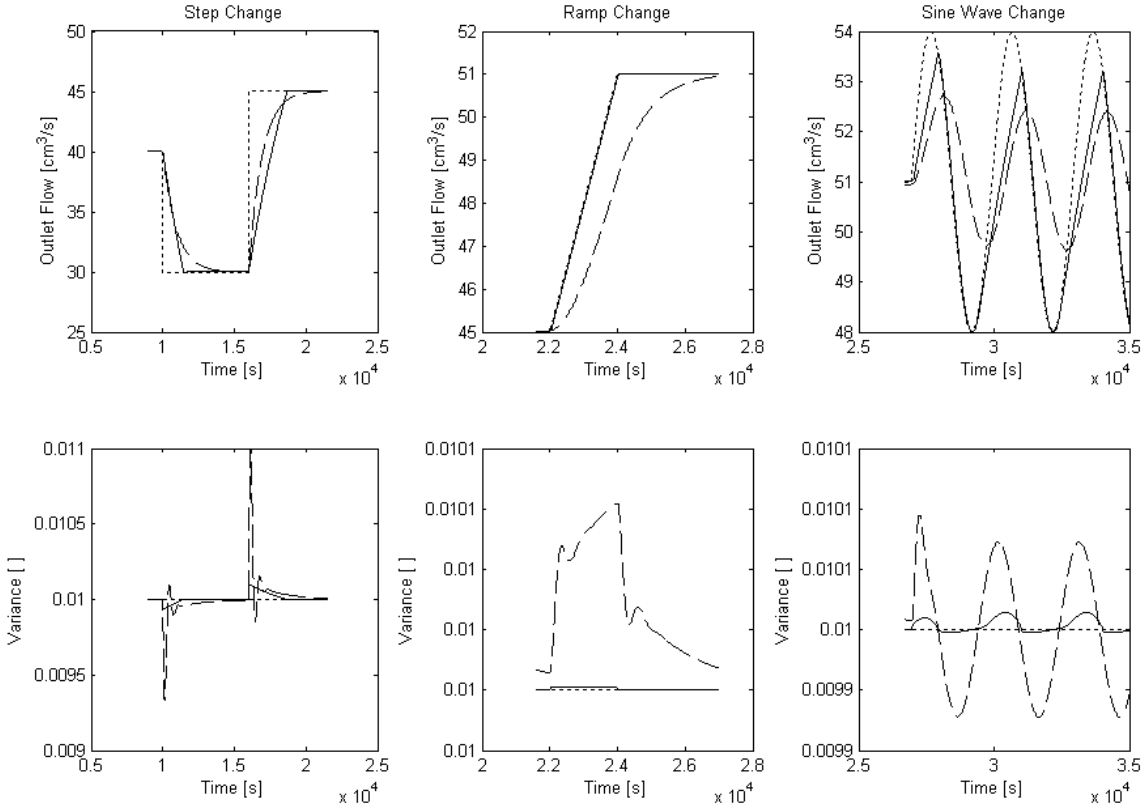

Figure VI.1 Closed-loop response and effects over Θ to set-point changes in F_o. Set-Point (dotted), MPC (solid), Multivariable PI (dashed).

For a ramp change in F_o at 0.003 $cm^3.s^{-1}/s$, the process variable controlled with MPC follows the ramp without deviations, compensating simultaneously the effect that this change has over Θ, while with the outlet flow PI controller occurs the classic change that implies that after an initial transient period the ramp input yields a ramp output, in addition to produce a light effect smaller to 1% over Θ that is compensated by variance PI controller.

For sine wave change in F_o with amplitude 3 cm^3/s and frequency 0.0021 rad/s, the MPC controller has the robustness to force the process variable to follow the trajectory of set-point with the same phase. Over Θ, again MPC controller is more accurate for reject the effect of set-point change in F_o.

In the three cases, it can be confirmed that no exist severe interactions between the two controlled variables, that is changes in set-point of F_o, do not produce high variations in Θ.

VI.2.2 Set-point changes in Θ

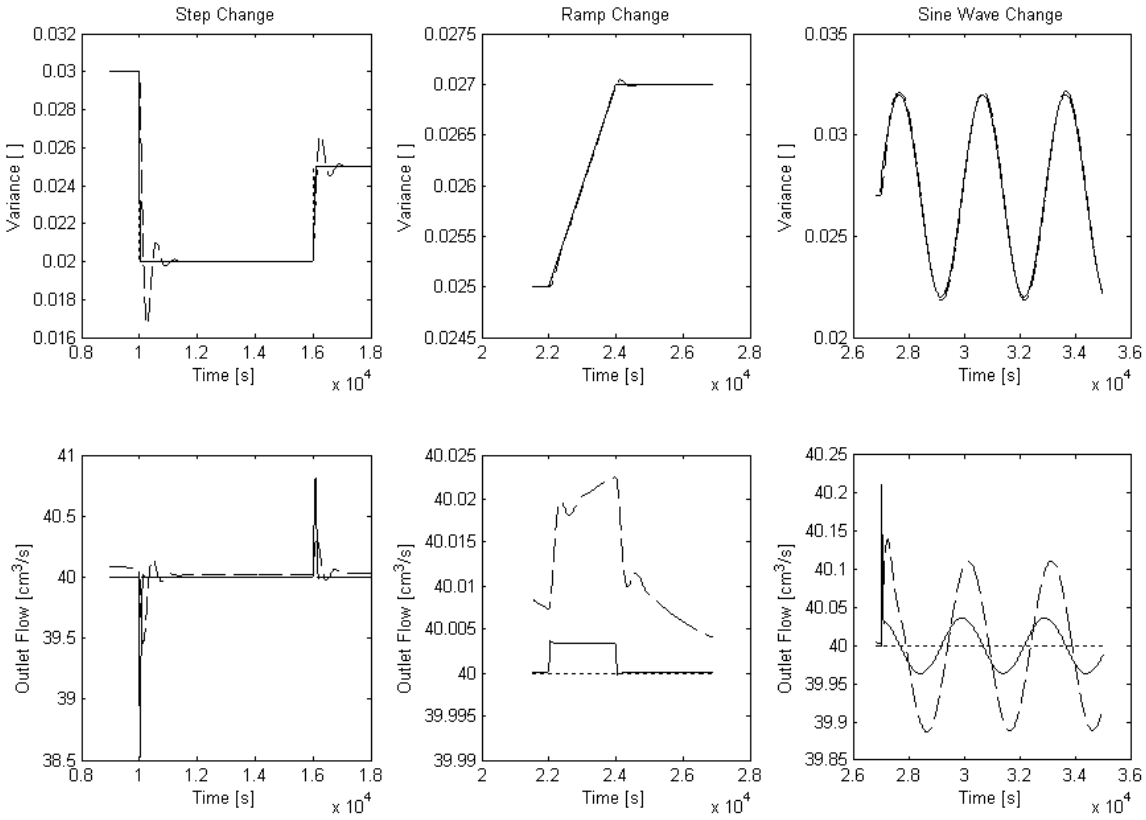

Figure VI.2 Closed-loop response and effects over F_o to set-point changes in Θ. Set-Point (dotted), MPC (solid), Multivariable PI (dashed).

Figure VI.2 depict the closed-loop response to set-point changes. For two step changes in Θ from 0.03 to 0.02 and 0.02 to 0.025, the MPC controller follows the trend without deviations, while with variance PI controller the decay ratio is 13% approximately. The variation in F_o produced by the changes in Θ is quickly compensated by MPC controller, while with outlet flow PI controller the stabilization is three times slower.

For a ramp change in Θ at $1x10^{-6}$/s and sine wave change with amplitude 0.005 and frequency 0.0021 rad/s, both controllers follow the same trajectory of set-point, and similarly to previous section, changes in set-point of Θ do not produce high variations in F_o.

VI.3 **Disturbance changes**

The case of disturbance changes is also referred to as the *regulator problem*. Again, while the load disturbances of a manipulated variable were eliminated, a disturbance set was loaded over other manipulated variable to study the performance of the controllers.

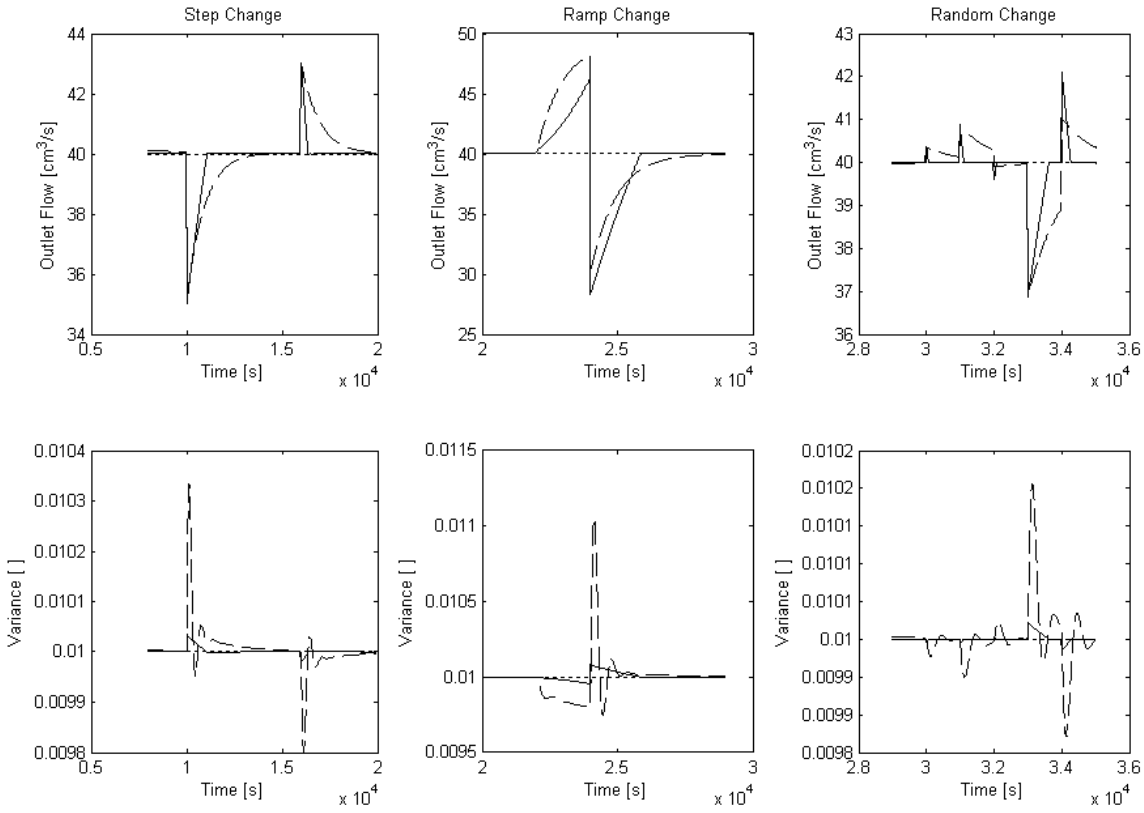

Figure VI.3 Closed-loop response and effects over Θ to load disturbances in F_o. Set-Point (dotted), MPC (solid), Multivariable PI (dashed).

Figures VI.3 and VI.4 depict the closed-loop response to load disturbances on F_o and Θ, respectively. In all cases, MPC controller always showed better levels of response to reestablish the process variables to their desired values.

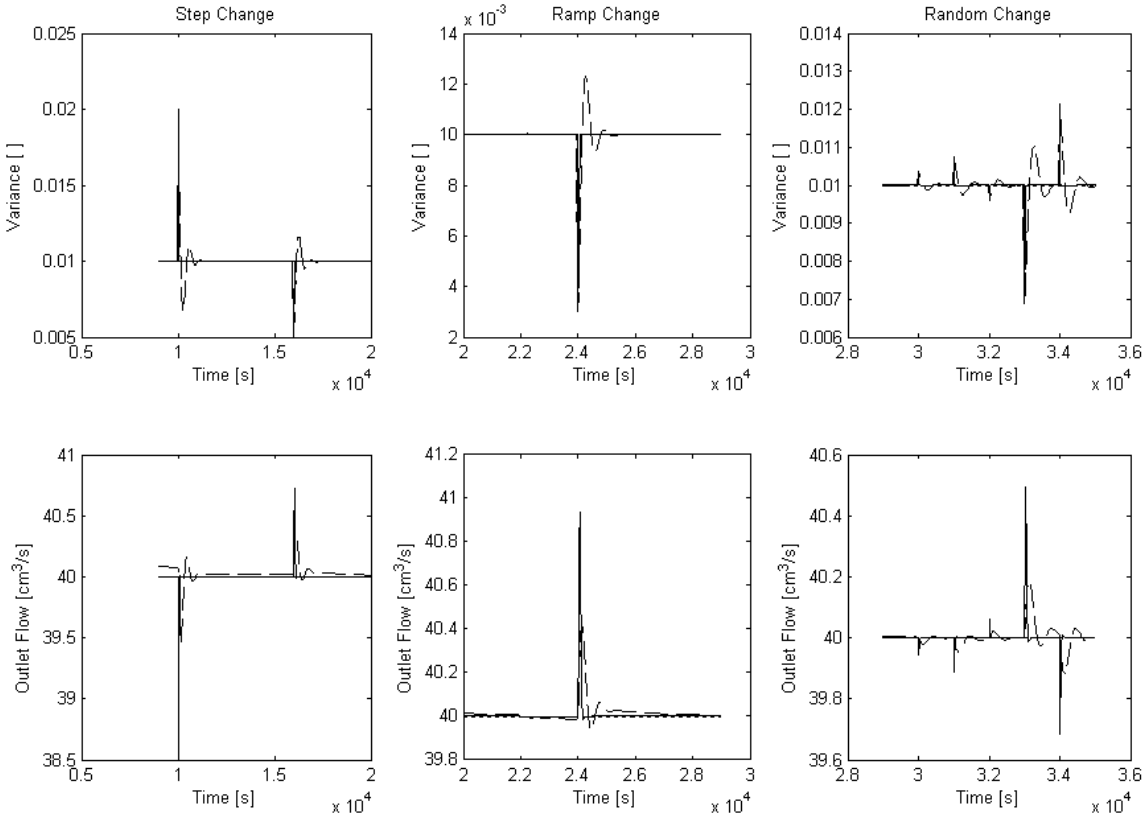

Figure VI.4 Closed-loop response and effects over F_o to load disturbances in Θ. Set-Point (dotted), MPC (solid), Multivariable PI (dashed).

VI.4 **Simultaneous changes**

To verify the stability and performance of the controllers was simulated the close loop response in Simulink® with a simulation time of 40 000 seconds and the following changes in the variables:

- Set-Point in Outlet Flow:

Table VI.1 Set-point change of outlet flow.

Time [sec]	Final Value [cm^3/s]	Change Type
0	40	---
10 000	30	Step
16 000	45	Step
22 000	0.003 sec^{-1}	Ramp
24 000	51	---
27 000	$3*\sin(2*\pi*2.1x10^{-3})$	Sine Wave
35 000	48.2	---

- Load Disturbance (noise) over Outlet Flow:

Table VI.2 Load disturbance over outlet flow.

Time [sec]	Random [cm^3/s]	Change Type
0	+/- 0.1	Frequency 100 sec
35 000	+/- 0.1	Frequency 100 sec

- Set-Point in Variance:

Table VI.3 Set-point change of variance.

Time [sec]	Final Value [ ]	Change Type
0	0.03	---
10 000	0.02	Step
14 000	0.025	Step
20 000	$1x10^{-6}$ sec^{-1}	Ramp
23 000	$0.005*\sin(2*\pi*2.1x10^{-3})$	Sine Wave
30 000	$2x10^{-6}$ sec^{-1}	Ramp
35 000	0.0178	---

- Load Disturbance (noise) over Variance:

Table VI.4 Load disturbance over variance.

Time [sec]	Random [ ]	Change Type
0	+/- 1e-7	Frequency 150 sec
35 000	+/- 1e-7	Frequency 150 sec

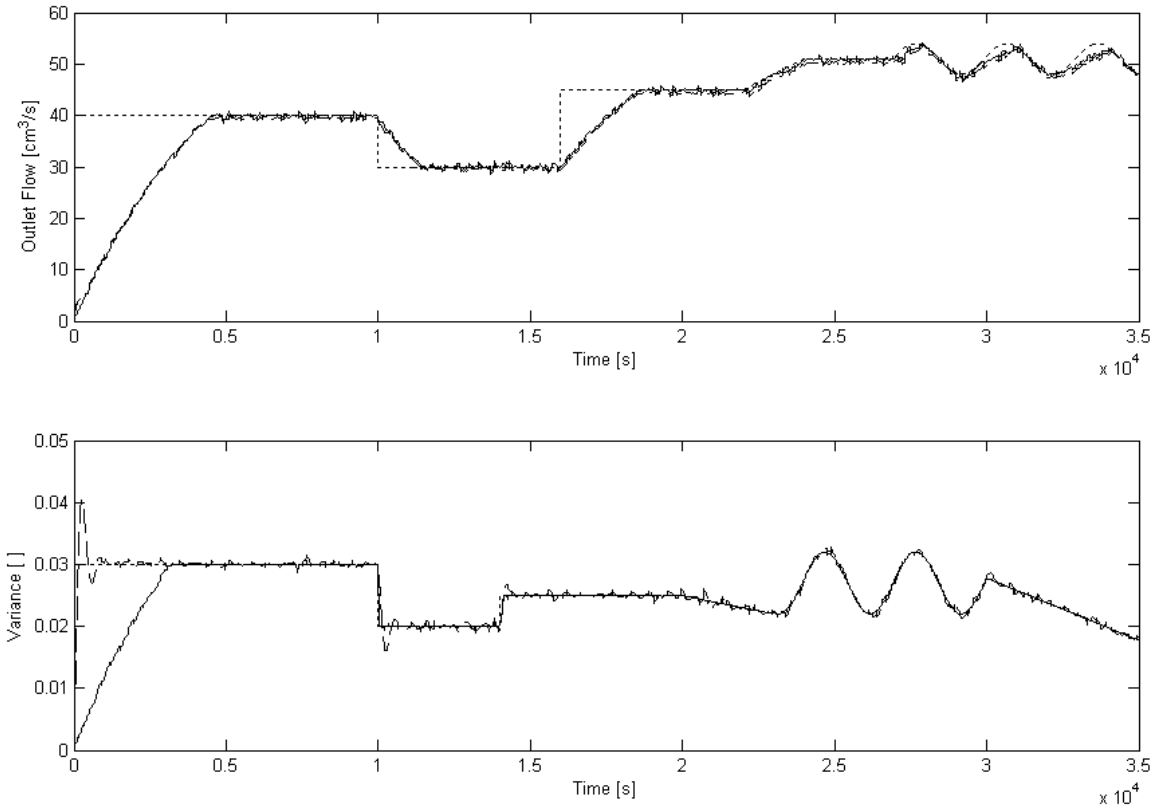

Figure VI.5 Closed-loop response for F_o and Θ. Set-Point (dotted), MPC (solid), Multivariable PI (dashed).

As can be seen in Figure VI.5 both controllers produce similar closed-loop responses for outlet flow. This is corroborated in Figure VI.6, which depicts the difference between set-point and process variable *error* for the changes described above. For control of variance, MPC controller is slower to reach the steady state, but it does not generate overshoots in the process variable after a step change in set-point, contrary to the effect of the PI controller.

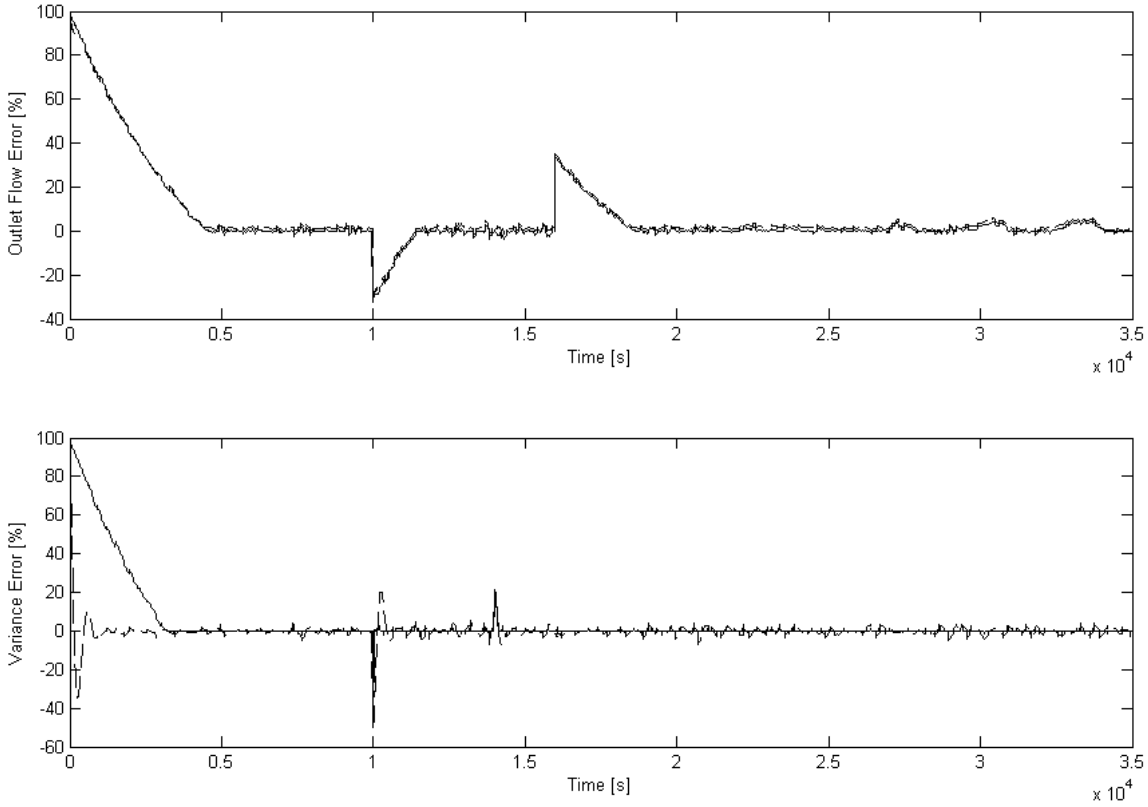

Figure VI.6 Error percent in closed-loop response for F_o and Θ. MPC (solid), Multivariable PI (dashed).

VI.5 **Robustness test**

The final test of the controllers developed was a robustness test. The performance of the controller system must be checked when the values of the process parameters deviate from the estimated nominal values, maintaining the adjustment parameters. In this case, first it was investigated only the effect of uncertainties in the output matrix $\mathbf{C}$, and next it was added the effect of uncertainties in the state matrix $\mathbf{A}$. To represent these uncertainties, Eqs. (IV.9) and (IV.11) are modified as:

$$\mathbf{A} = \begin{bmatrix} -0.0002 & 0 & 0 & 0 & 0 \\ 0 & -0.0006 & 0 & 0 & 0 \\ 0 & 0 & -0.0183 & 0 & 0 \\ 0 & 0 & 0 & -0.0025 & -0.0004 \\ 0 & 0 & 0 & 0.0039 & 0 \end{bmatrix} \qquad \text{(VI.1)}$$

and

$$\mathbf{C} = \begin{bmatrix} 0.0128 & 0 & -0.2228 & 0 & 0 \\ 0 & 0.00038 & 0 & -0.01111 & -0.00152 \end{bmatrix} \qquad \text{(VI.2)}$$

Figure VI.7 depicts the case of 5% decrease in values of matrix $\mathbf{C}$, that is the description of the vector of system's outputs. Figure VI.8 depicts the case described above adding a decrease in the element (2,2) of matrix $\mathbf{A}$ from -0.0002 to 0.0006, that is an element of state that describe the system's dynamics. For MPC controller, Matrix $\mathbf{A}$ is part of the optimization function, Eq. (V.7), since it participates in the calculation of vector of measured outputs $\mathbf{y}_m(k)$ from the state vector of the plant $\mathbf{x}(k)$.

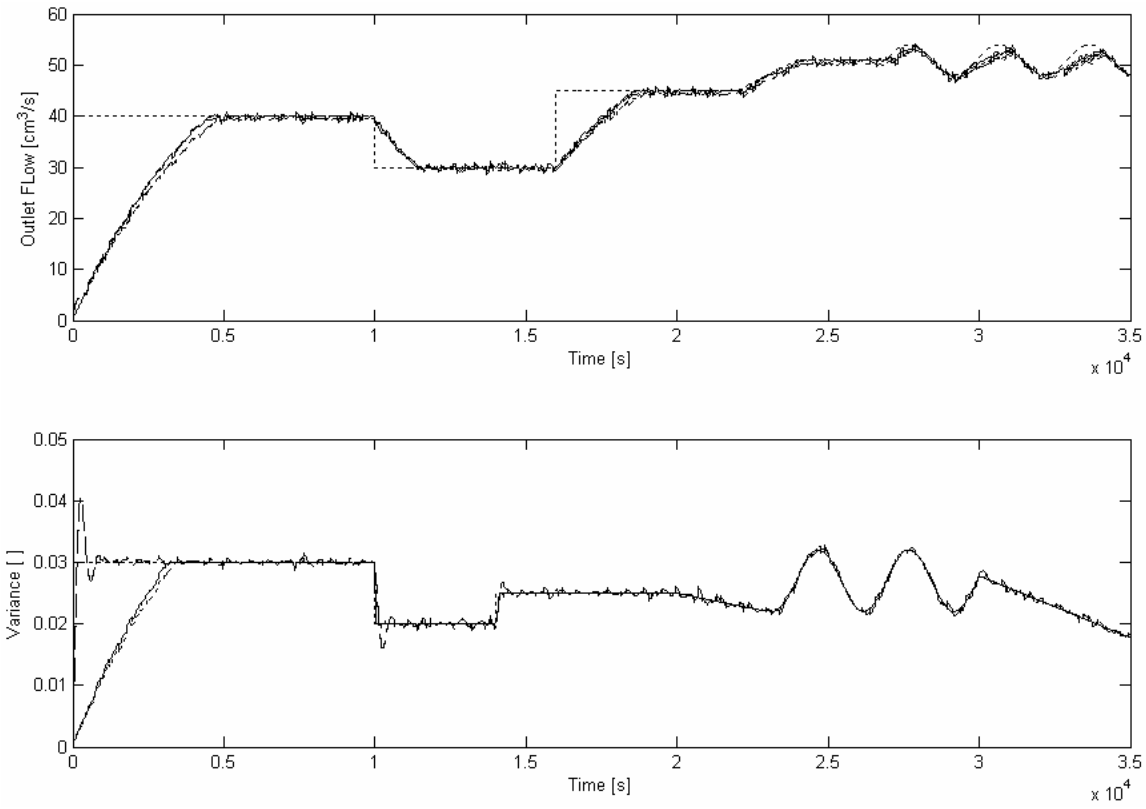

Figure VI.7 Robustness test in presence of uncertainties in matrix **C**. Set-Point (dotted), MPC with exact process model (solid), MPC with uncertain process model (dotted), Multivariable PI with exact process model (dashed), Multivariable PI with uncertain process model (dashdot).

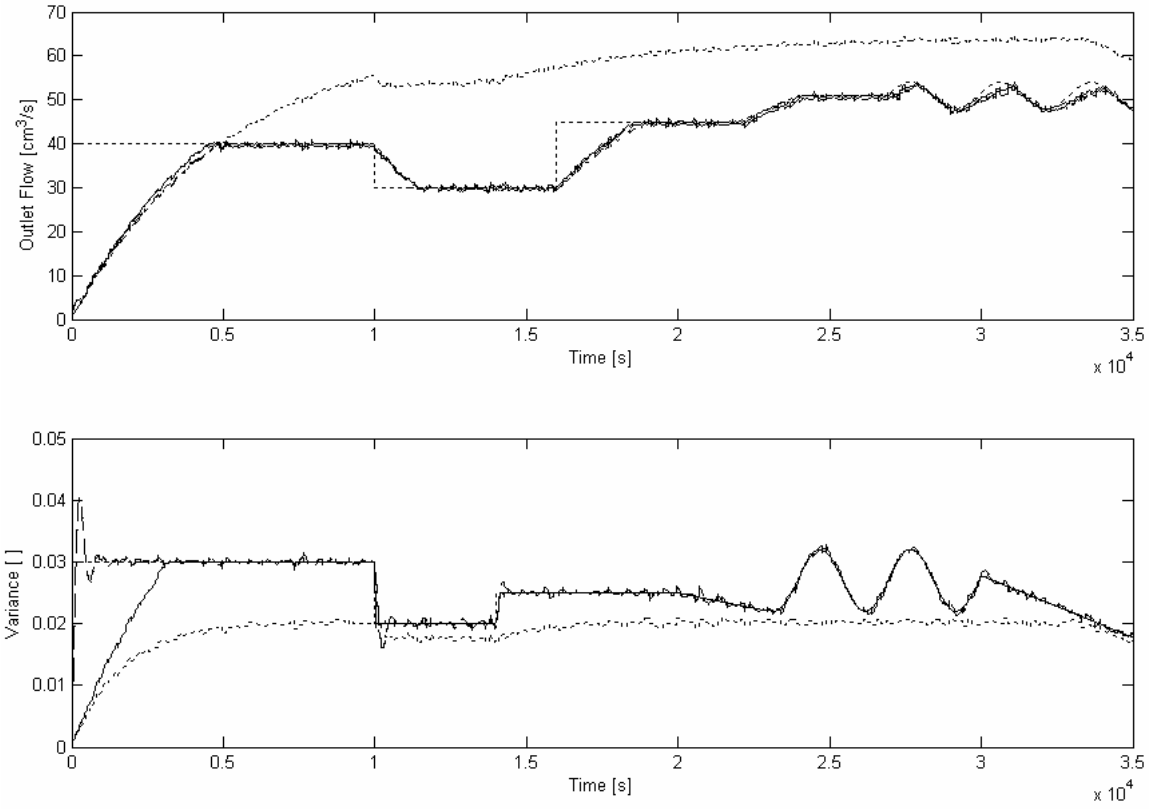

Figure VI.8 Robustness test in presence of uncertainties in matrices **A** and **C**. Set-Point (dotted), MPC with exact process model (solid), MPC with uncertain process model (dotted), Multivariable PI with exact process model (dashed), Multivariable PI with uncertain process model (dashdot).

For the test with uncertainties in the output matrix **C**, both controllers showed robustness, while adding uncertainties in the state matrix **A** caused that the close-loop response deteriorated under MPC. As can be seen in Figure VI.8, Multivariable PI controller has a good performance, while MPC is not able to handle adequately these changes in the model, since its optimum moves are based on the dynamics model.

CHAPTER VII: CONCLUSIONS AND RECOMMENDATIONS

VII.1 Conclusions

The objectives of this investigation were accomplished. A continuous rotating powder mixing was modeled. The specific objectives were realized:

- An ideal model was developed to describe a continuous rotating powder mixer.
- Two feedback control strategies (PI, MPC) were developed for a continuous rotating powder mixer, where the mixer dynamics is described by the model developed above.
- Last but not least implementation of the model through Simulink by Matlab allowed to compare the robustness, overshoots on set-point tracking, performance and capacity to reject the effect of load disturbances of the strategies developed.

Two multivariable control strategies PI and MPC were developed to control a continuous tumble mixer of granular materials. Both strategies were based on a semi-empirical model, whose input variables are the inlet flow of material to mix and the rotational velocity of the mixer, while the output variables are the material outlet flow from the mixer and the variance of mixing.

A contribution of this research was the development of a semi-empirical model, in which assumptions were incorporated that the powder level variation inside the mixer has the same behavior of a Newtonian liquid discharging from an orifice by the effect of the gravitational force, and that the densities of noncohesive granular materials are similar and remain constant during the mixing process. This component of the model was coupled with an exponential expression for the behavior of variance of mixing as a function of fill level inside the mixer and its rotational velocity. The results showed that

the trends of the output variables obtained from the semi-empirical model are consistent with expected behavior observed by other authors in batch mixers.

The time domain semi-empirical model developed is nonlinear with the largest nonlinearity in the outlet flow. Linear transformations through an analysis of parameter estimation on Laplace domain and state-space representation show a better agreement for the variance behavior than for outlet flow. The control strategies designed are based on these linear mathematical models.

In the design of the multivariable control PI strategy, a RGA analysis does not indicate severe interactions between manipulated and controlled variables, suggesting that it was not necessary to consider the use of decoupling control. The tuning of PI controllers was based on the fact that the transfer function that relate $F_o(s)$-$F_i(s)$ is much slower than the transfer function that relate $\Theta(s)$-$M(s)$, forestalling that the first loop stability was affected by the change in closed-loop process gain.

MPC control strategy was developed incorporating hard constraints on inputs, simulating the limits imposed by the final control elements of the system. In the state feedback control law associated with MPC, it was used a weight vector on outputs system that penalizes deviations from its set-point. The corresponding element to $\Theta(k)$ in this vector was greater than that of $F_o(k)$, by an order of magnitude of $1x10^4$. This forced the controller to have a priority on stability and performance on the variance of mixing. However this large w value for $\Theta(k)$ sacrifices slightly the stability of $F_o(k)$.

For set-point tracking in both F_o and Θ, MPC controller does not present oscillations and overshoots. In the control of variance, MPC controller was slower to reach the steady state than PI, but it did not generate overshoots, contrary to the PI controller. Multivariable PI controller had better performance when the state matrix into

state-space representation of the process was modified, confirming its robustness. On the other hand MPC could not handle these changes in the model.

Based on the conditions and assumptions used in this work, the simulation results show that the proposed strategies are valid and provide a reliable control. The multivariable PI showed an adequate robustness.

VII.2 **Recommendations**

For the implementation on a continuous tumble mixer of two control strategies developed in this research, it is necessary to use an on-line image analysis in order to determine the variance of mixing and a sensor for outlet flow of material from the mixer. As final control elements, a motor connected to a driver and two feed systems with a ratio controller for compounds A and B to mix. For the data acquisition in order to propose the empirical model of mixing, configuration and commissioning of the MPC or Multivariable PI strategies, a *Distributed Control System* (DCS) would prove to be a suitable control architecture, especially if the decision is to implement the MPC controller in which the computational expense associated with solving the QP on-line can be inconvenient.

Due to the absence of mixing models in continuous tumbles based in fundamental equations, and because the mixing problem is treated as a statistical or stochastic process, new control schemes such as *Fuzzy Logic* (FL) control strategy could be explorer for the control of these mixers. This technique provides a simple way to arrive at a definite conclusion based upon vague, ambiguous, imprecise, noisy, or missing input information.

REFERENCES

[1] F. J. Muzzio, T. Shinbrot, B. J. Glasser. Powder technology in the pharmaceutical industry: the need to catch up fast, *Powder Technology* **124** (2002) 1-7.

[2] S. Muerza, H. Berthiaux, S. Massol, G. Thomas. A dynamic study of static mixing using on-line image analysis, *Powder Technology* **128** (2002) 195-204.

[3] Batch Systems Standards: ANSI/ISA-88.01-1995, ANSI/ISA-88.00.02-2001, ANSI/ISA-88.00.03-2003, ISA-TR88.0.03-1996, *ISA – The Instrumentation, Systems, and Automation Society*. http://www.isa.org.

[4] F. Zhao, W. Du, G. Yu. An improved generalizad analytical predictor for chemical process control, *Journal of Process Control* **9** (1999) 185-191.

[5] D. E. Seborg, T. F. Edgar, D. A. Mellichamp. *Process Dynamics and Control*, 2d ed., John Wiley & Sons, Inc., New Jersey, 2004.

[6] L. T. Fan, Y. M. Chen. Recent developments in solids mixing, *Powder Technology* **61** (1990) 255-287.

[7] K. Malhotra, A. S. Mujumdar. Fundamental particle mixing studies in an agitated bed of granular materials in a cylindrical vessel, *Powder Technology* **55** (1998) 107-114.

[8] Y. Kaneko, T. Shiojima, M. Horio. Numerical analysis of particle mixing characteristics in a single helical ribbon agitator using DEM simulation, *Powder Technology* **108** (2000) 55-64.

[9] J. J. McCarthy, D. V. Khakhar, J. M. Ottino. Computational studies of granular mixing, *Powder Technology* **109** (2000) 72-82.

[10] J. J. McCarthy. Micro-modeling of cohesive mixing processes, *Powder Technology* **138** (2003) 63-68.

[11] M. Aoun-Habbache, M. Aoun, H. Berthiaux, V. Mizonov. An experimental method and a Markov chain model to describe axial and radial mixing mixing in a hoop mixer, *Powder Technology* **128** (2002) 159-169.

[12] J.J. McCarthy, T. Shinbrot, G. Metcalfe, J. E. Wolf, J.M. Ottino. Mixing of granular materials in slowly rotated containers, *AIChE Journal* **42** (1996) 3351-3363.

[13] T. Elperin, A. Vikhansky. Kinematics of the mixing of granular material in slowly rotating containers, *Europhysics Letters* **43** (1998) 17-22.

[14] M. Moakher, T. Shinbrot, F.J. Muzzio. Experimentally validated computations of flow, mixing and segregation of non- cohesive grains in 3D tumbling blenders, http://www.muzzio.rutgers.edu/OnlinePapers/MDPaper.pdf.

[15] AJAX Equipment. Ajax LunFlow™ Continuous Mixer, http://www.ajax.co.uk/conmix.htm.

[16] D.V. Khakhar, J.J. McCarthy, J.F. Gilchrist, J.M. Ottino. Chaotic mixing of granular materials in two-dimensional tumbling mixers, *Chaos* **9** (1999) 195-205.

[17] K. Ogata. *Modern Control Engineering*, 4th ed., Prentice Hall, New Jersey, 2002.

[18] T. E. Marlin. *Process Control: Designing Processes and Control Systems for Dynamic Performance*, McGraw-Hill, Inc., New York, 1995.

[19] D.E. Rivera, M. Morari, S. Skogestad. Internal Model Control. 4. PID Controller Design, *Ind. Eng. Process Design Dev.*, **25** (1986) 252.

[20] J.G. Van Antwerp, R.D. Braatz. Model predictive control of large scale processes, *Journal of Process Control* **10** (2000) 1-8.

[21] C.V. Rao, J.B. Rawlings. Linear programming and model predictive control, *Journal of Process Control* **10** (2000) 283-289.

[22] A. Bemporad, M. Morari, N.L. Rocker. *Model Predictive Control Toolbox for use with Matlab®*, The MathWorks, Inc., Natick, MA, 2005.

[23] A. Bemporad, M. Morari, V. Dua, E.N. Pistikopoulos. The explicit solution of Model Predictive Control via Multiparametric Quadratic Programming, *Proceedings of the American Control Conference*, Chicago, Illinois, 2000.

APPENDIX

A. Definition of semi-empirical models of mixing in Simulink by Matlab

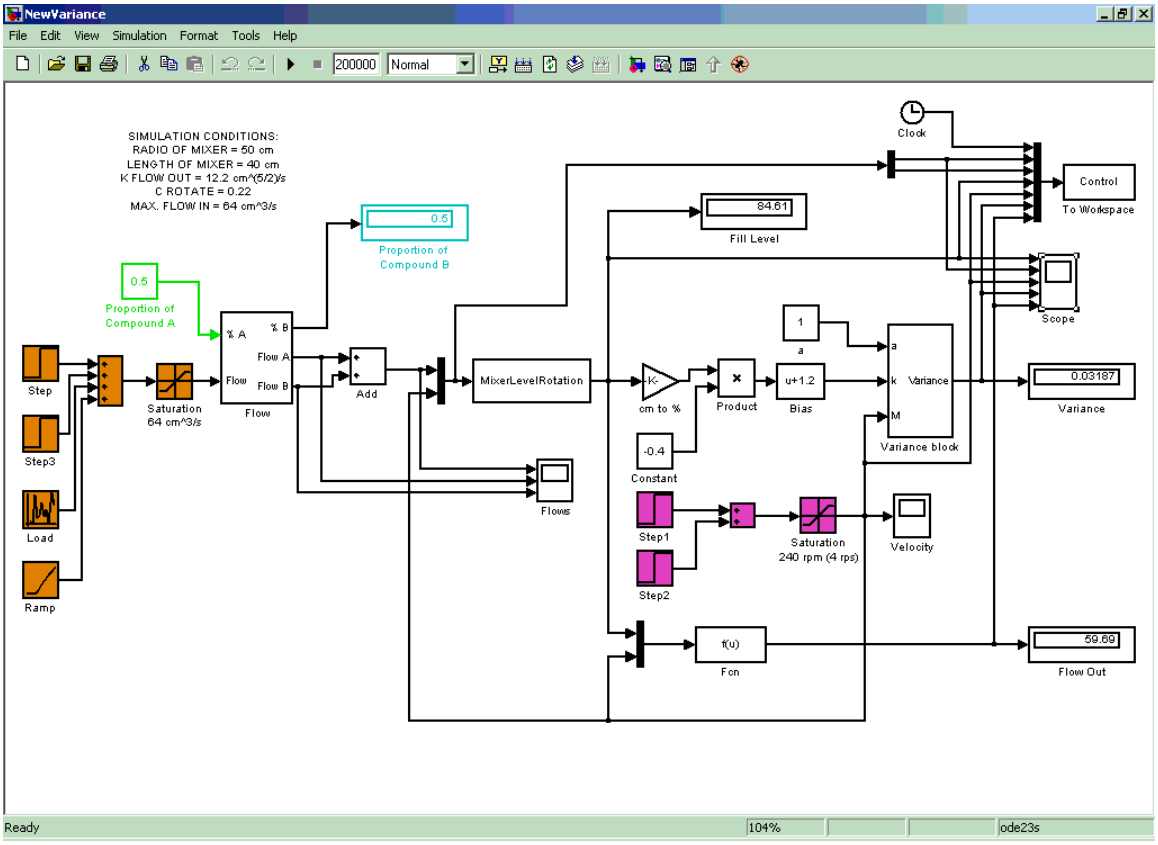

B. Definition of transfer functions system in Matlab

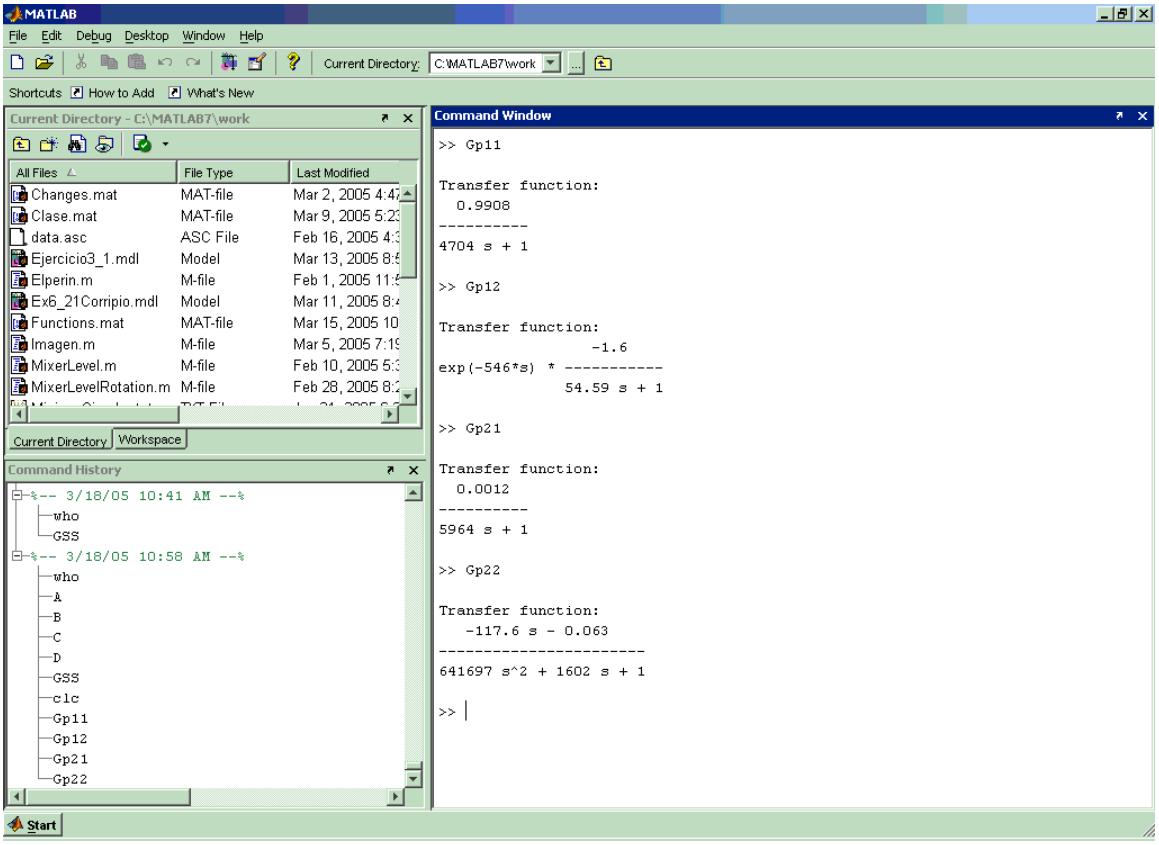

C. MIMO 2X2 system in Matlab

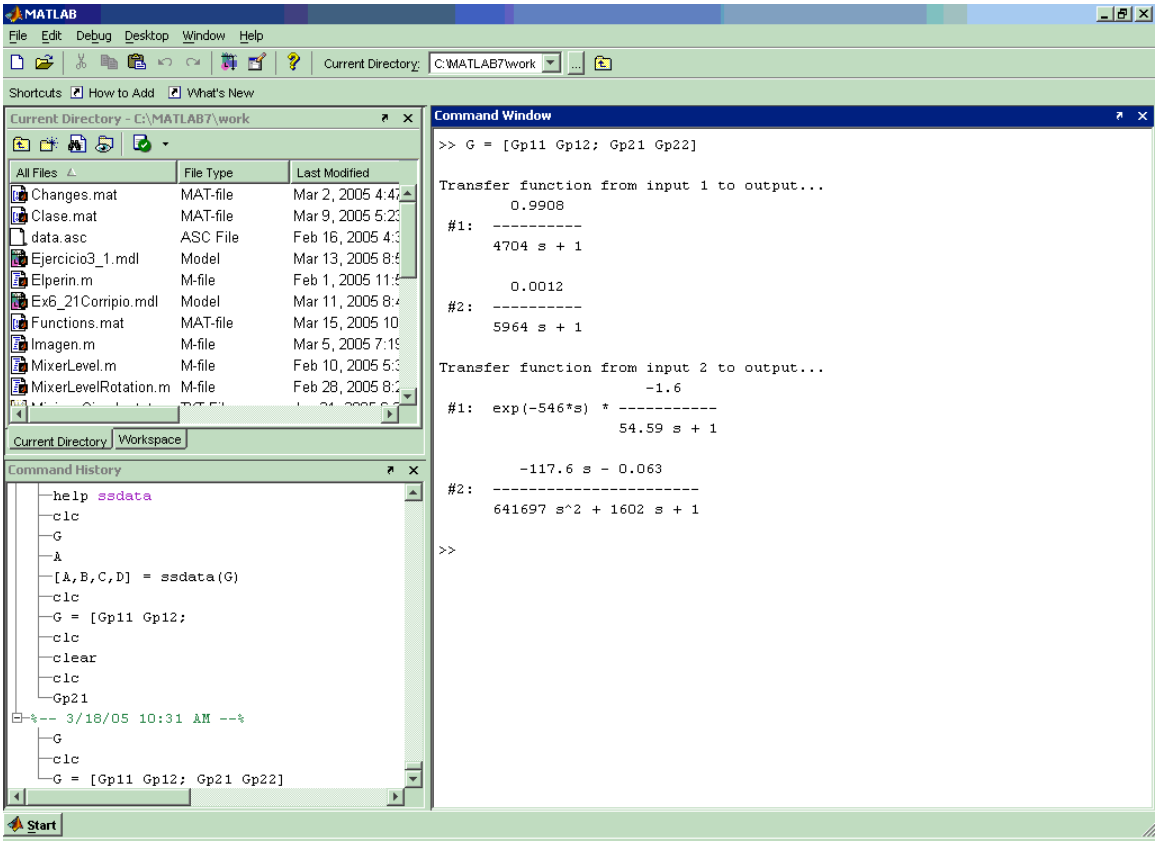

D. Conversion from MIMO 2X2 system to state-space system

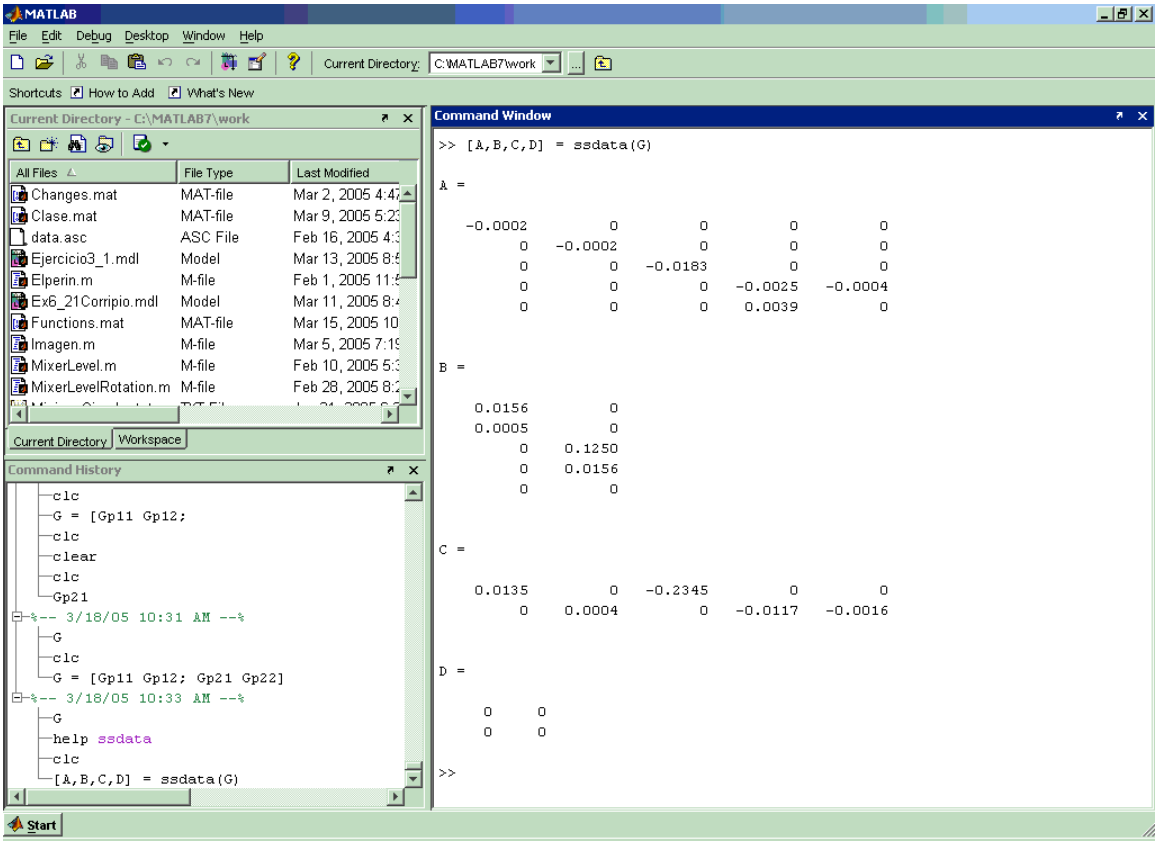

E. Definition of state-space system in Matlab

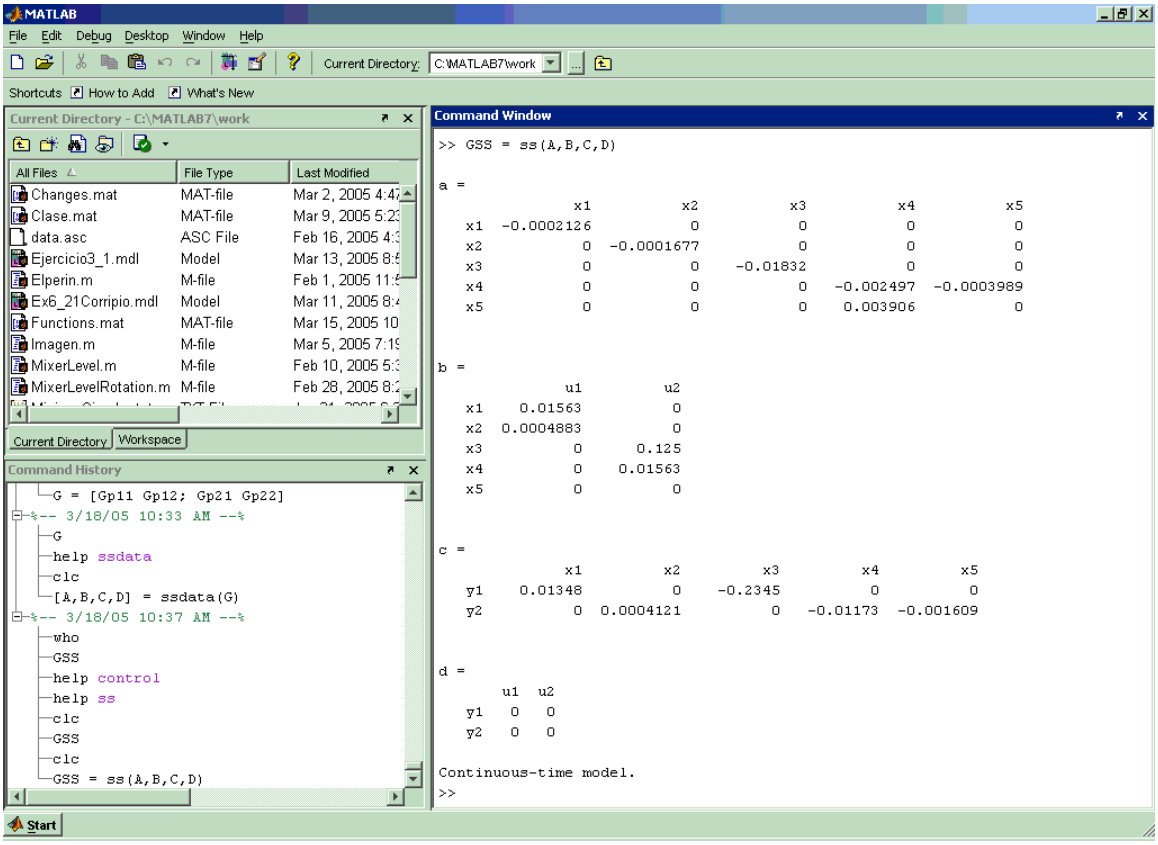

F. PI system control over Laplace domain in Simulink by Matlab

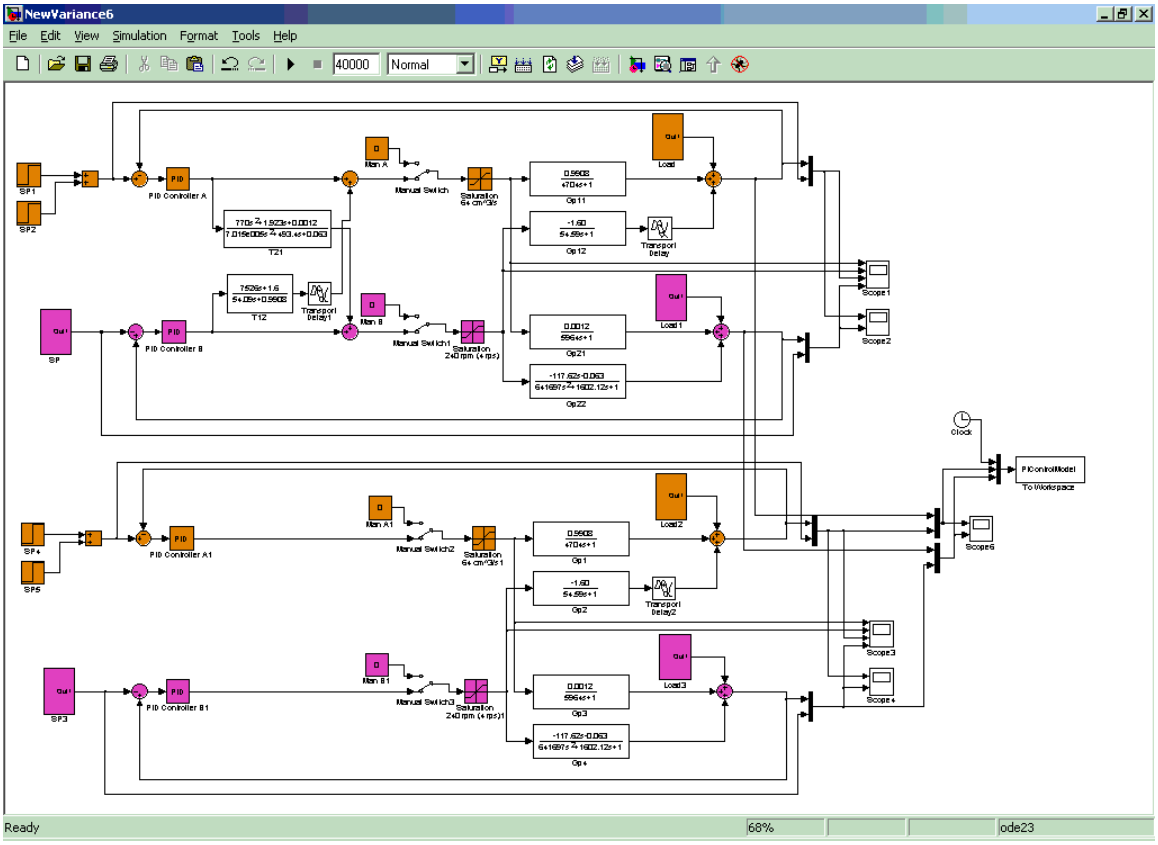

G. PI system control over time domain in Simulink by Matlab

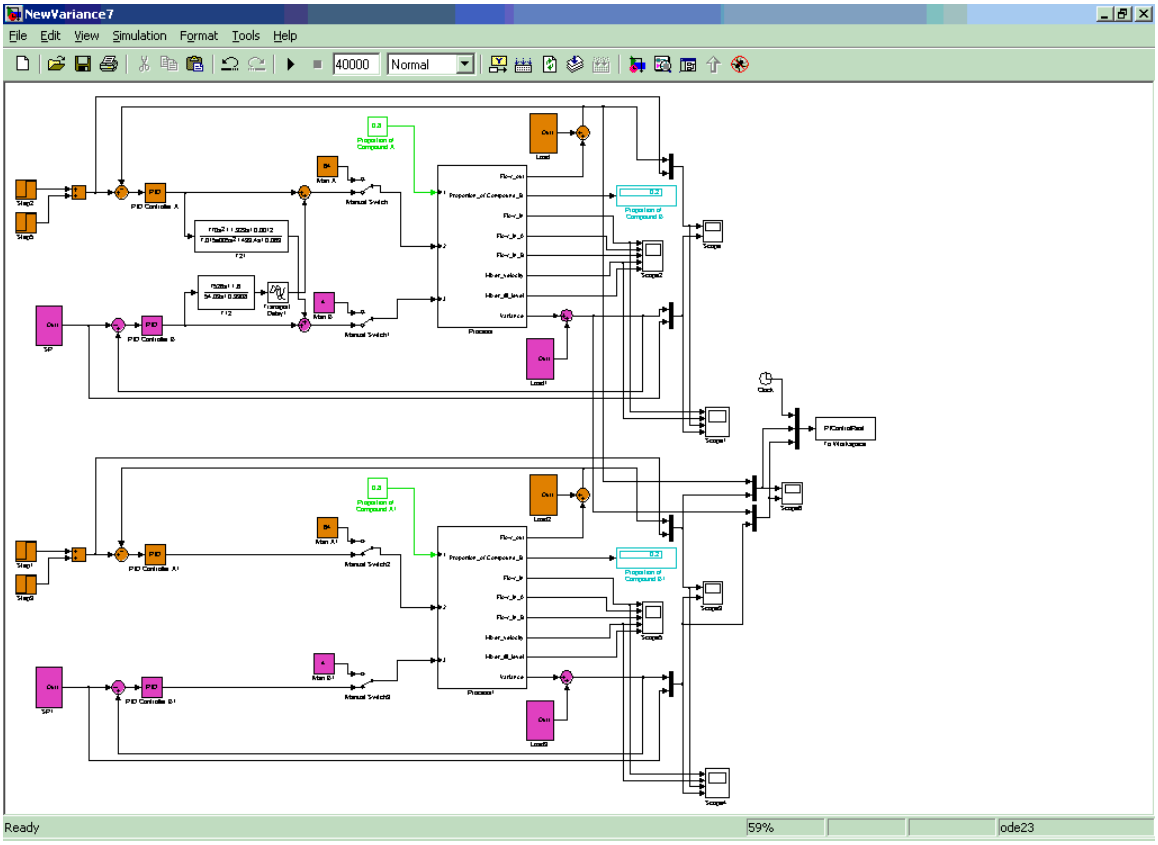

H. Comparison between PI system control with and without decouplers over time domain

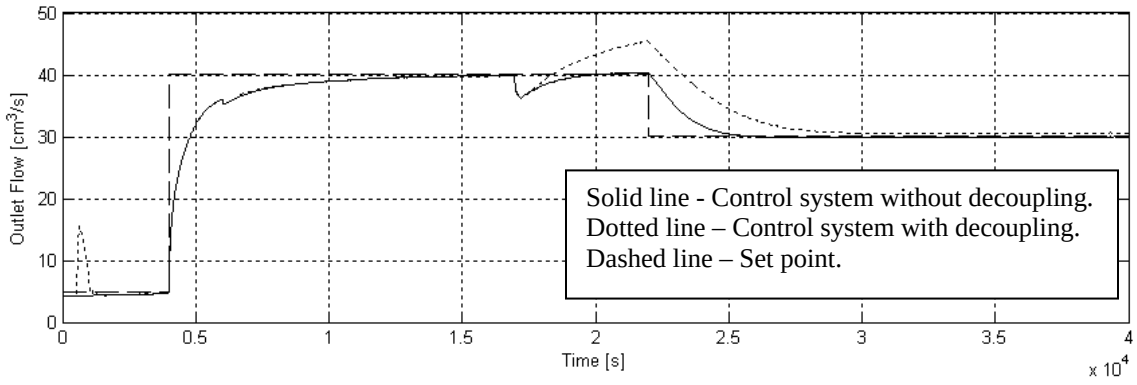

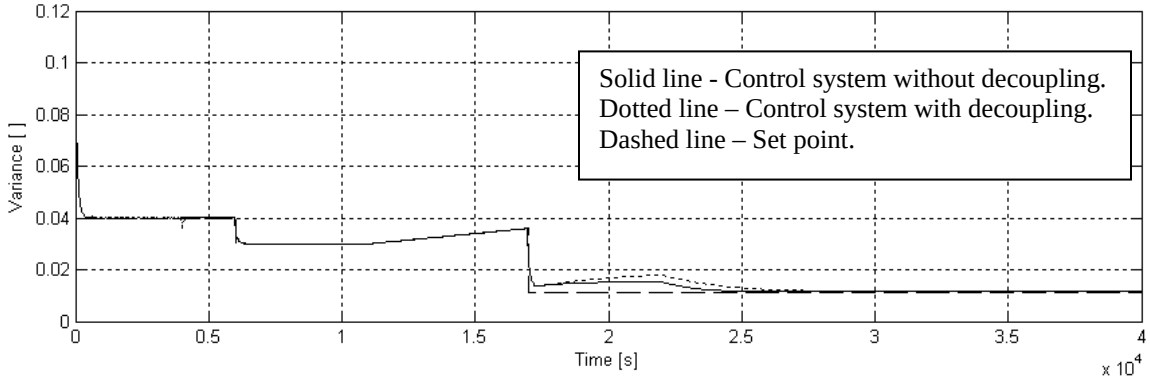

I. Block diagram for model predictive control

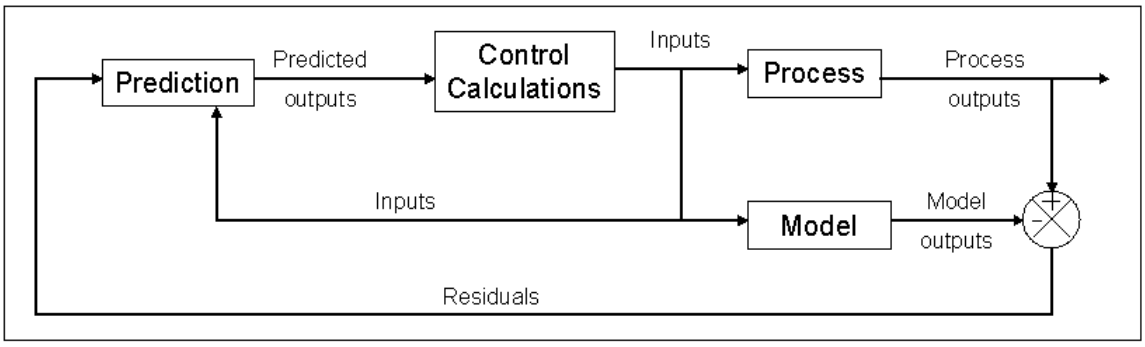

J. MPC system control over continuous tumble mixer in Simulink by Matlab